Joint Trajectory and Resource Optimization for Delay minimization of UAV-Enabled NOMA-MEC System with LWPT

Xuecai Bao, *Member, IEEE,* Fugui Liu, Fenghui Zhang, *Member, IEEE,* Kun Yang, *Fellow, IEEE,*

***Abstract*—Unmanned aerial vehicles (UAVs) enhance mobile edge computing (MEC) coverage, but in remote emergency scenarios limited battery life and scarce spectrum exacerbate interference, link instability, and end-to-end delay. To address these issues, we propose a joint trajectory and delay-minimization framework that integrates laser-beamed wireless power transfer (LWPT) with UAV-enabled non-orthogonal multiple access (NOMA) MEC. First, we present a practical system architecture where a ground laser-powered beacon (PB) continuously recharges the UAV during flight, enabling persistent aerial patrols that concurrently offer wireless charging and computation services to ground users. Second, we formulate a unified mixed-integer nonconvex optimization problem that jointly optimizes the UAV trajectory, task offloading ratios, PB power distribution, and user-scheduling policy under energy-causality, NOMA interference, and flight-dynamics constraints. Third, to address the resulting non-convexity, we develop a hierarchical decomposition and alternating-optimization method: the original problem is decomposed into trajectory and resource-allocation subproblems and solved using convex approximations and efficient scheduling algorithms to obtain practical solutions. Fourth, extensive simulations demonstrate that the proposed LWPT-assisted NOMA UAV-MEC scheme substantially reduces total system delay while improving energy efficiency and throughput compared with conventional OMA-MEC baselines and five recent heuristic algorithms.**

***Index Terms*—mobile edge computing (MEC), unmanned aerial vehicle (UAV), laser-beamed wireless power transfer (LWPT), non-orthogonal multiple access (NOMA), task offloading**

I. Introduction

THE rapid expansion of IoT-driven ecosystems, including smart cities, intelligent water management, natural disaster recovery, emergency response, remote environmental monitoring, and urban digital twins, has sharply raised the need for ultra-low-delay, high-performance computing at the network edge [1], [2]. In many of these scenarios, unmanned aerial vehicles (UAVs) stand out for real time aerial surveillance and on the fly route optimization, thanks to their exceptional mobility, flexible deployment, and strong line of sight links [3], [4]. When outfitted with mobile edge computing (MEC) nodes, UAVs can process data immediately where it is generated, supporting delay sensitive and bandwidth intensive tasks in critical contexts such as disaster relief, emergency response, and remote monitoring [5], [6].

However, practical implementation of UAV-MEC systems reveals three fundamental challenges: 1) Energy scarcity: UAV flight time and onboard compute power are limited by battery capacity, making long-duration missions impossible. 2) Dynamic workload: As task arrivals vary rapidly in dense user environments, complicating offload scheduling and creating a major bottleneck for massive concurrent access. 3) Strict delays: Mission critical applications impose tight delay bounds that conventional schemes struggle to meet [7]–[9].

Traditional orthogonal multiple access (OMA) and fixed batteries cannot simultaneously address these constraints. OMA fails to support massive users due to its orthogonal resource allocation, while fixed batteries limit endurance. As a result, system scalability and quality of service (QoS) suffer when serving large user bases or extended missions, highlighting the need for a new UAV-MEC design to improve spectrum utilization, extend energy endurance, and intelligently allocate resources within strict delay budgets. To mitigate these issues, researchers have employed non-orthogonal multiple access (NOMA) to enhance spectrum efficiency through simultaneous multi-user transmission in the power domain, in combination with radio frequency wireless power transfer (RF-WPT) to recharge UAVs mid-flight [10]–[13]. Nonetheless, RF-WPT experiences severe fading at typical UAV-to-ground distances, making it unsuitable for long-range missions [9]. Although laser beam wireless power transfer (LWPT) has been proposed to solve this fading problem [14][15], no existing study has integrated LWPT with uplink NOMA in a unified UAV-MEC framework. This combination is critical to simultaneously support massive concurrent access through NOMA's spectrum efficiency and long-duration endurance via LWPT's stable, high-density energy supply. Moreover, most existing optimization schemes only consider partial factors (e.g., trajectory or resource allocation) rather than synchronously optimizing flight trajectories, energy harvesting, resource allocation, and task scheduling under strict delay constraints, leaving a gap

This work was supported by the National Natural Science Foundation of China (Grant No. 61961026 and 61962036), China Postdoctoral Science Foundation(Grant No. 2020M671556).

Xuecai Bao is with the Jiangxi Province Key Laboratory of Smart Water Conservancy, Jiangxi University of Water Resources and Electrie Power, Nanchang 330099, China, and also with College of Telecommunications and Information Engineering, Nanjing University of Posts and Telecommunications, Nanjing 210003, China.(e-mail: lx97821@juwp.edu.cn/lx97821@nit.edu.cn).

Fugui Liu is with the Jiangxi Province Key Laboratory of Smart Water Conservancy, Jiangxi University of Water Resources and Electrie Power, Nanchang 330099, China.(e-mail: fugui_liu2023@163.com).

Fenghui Zhang is with the School of Information Science and Engineering, Southeast University, Nanjing, 211189, China, also with School of Electronics & Information Engineering, West Anhui University, Lu'An 310014, China.(e-mail: 03000072@wxc.edu.cn).

Kun Yang is with the School of Computer Science & Electronic Engineering, University of Essex, London, CO4 3SQ, UK.(e-mail: kunyang@essex.ac.uk).

in meeting the tight delay bounds required for mission-critical applications where even minor delays can compromise operational success.

To fill these gaps, we propose the first unified UAV-MEC framework that integrates uplink NOMA with laser-based wireless power transfer (LWPT). Our framework enables simultaneous multiuser access (via NOMA) and continuous energy replenishment (via LWPT), while a synchronous optimization algorithm minimizes total service delay by jointly optimizing flight trajectories, energy harvesting, resource allocation, and task scheduling.

To achieve this, we formulate the problem as a mixed-integer nonconvex optimization problem that jointly optimizes UAV trajectory planning, user scheduling, computation offloading ratios, and laser transmission power, subject to constraints on energy harvesting efficiency, UAV flight dynamics, and strict delay bounds. Recognizing the intractability of the original nonconvex problem, we apply mathematical transformation techniques (e.g., convex relaxation and successive convex approximation) to reformulate it into a tractable convex form, ensuring near-optimal performance while reducing computational complexity. This integrated approach not only fills the gap in combining LWPT and uplink NOMA into a unified UAV-MEC framework but also addresses the lack of synchronous multi-factor optimization under strict delay constraints, laying the groundwork for our key contributions summarized below.

1) We propose a UAV-assisted MEC architecture that deeply integrates laser wireless power transfer (LWPT) with uplink non-orthogonal multiple access (NOMA) to address delay in high-density monitoring of remote areas. Combining LWPT's long-range wireless charging, NOMA's spectrum reuse, and MEC's computing capabilities, the framework enhances spectrum efficiency, computing power, and endurance. Unlike existing studies that treat energy transfer, communication, and computing separately, our unified design integrates physical-layer energy transfer with network-layer resource scheduling, offering a practical and theoretically sound solution for UAV deployment in disaster response and emergency communications.
2) We propose a joint optimization model that simultaneously optimizes UAV trajectory, user scheduling, task offloading ratio, and laser power allocation to minimize system delay under energy-harvesting, flight-dynamics, and NOMA interference constraints. By exploiting the directionality of laser wireless power transfer and enforcing energy-causality constraints to ensure sustainable energy for the UAV and ground devices, the model reveals strong coupling among power, computation resources, and trajectory. This substantially improves optimization accuracy and practicality compared to per-module approaches.
3) We propose a hierarchical iterative algorithm combining problem decomposition with successive convex approximation (SCA). The UAV trajectory and user-association matrix are discretized to reduce complexity while explicitly modeling mobility, channel, interference, and energy-harvesting dynamics. The original problem is split into a joint offloading-and-power subproblem and a trajectory subproblem, convexified via first-order Taylor expansions. The algorithm is customized for the LWPT–NOMA coupling and outperforms generic alternating-optimization frameworks.
4) We evaluated the proposed scheme under various network conditions using metrics such as system delay and UAV flight trajectory. Results demonstrate its clear superiority over benchmark schemes in convergence speed, computational efficiency, and optimization accuracy.

The rest of the paper is organized as follows. Section II reviews related work. Section III presents the system model and problem formulation. Section IV details our joint user-scheduling and optimization framework. Section V shows simulation results. Section VI concludes and outlines future research.

II. Related Work

UAVs offer high mobility and rapid deployment capabilities, enabling them to temporarily host Mobile Edge Computing (MEC) servers in regions with underdeveloped ground infrastructure. Their cost-effectiveness and on-demand deployment further facilitate flexible network expansion. NOMA enhances resource utilization efficiency, supporting concurrent computational task offloading for a larger user base, mitigating resource contention in high-density scenarios, and boosting system throughput and service concurrency. WPT enables continuous energy supply from the network edge to mobile devices, alleviating the bottleneck caused by the tension between escalating computational demands and constrained device energy, thereby significantly improving service availability and sustainability in emergency response and remote coverage scenarios. Consequently, research on MEC networks integrating UAVs, NOMA, and WPT has emerged as a key direction for enhancing energy efficiency and overall service quality. In this section, we systematically review the technological evolution and recent advances in this domain, discuss remaining challenges, and identify gaps in existing theoretical frameworks, such as closed-loop energy management, delay guarantees, coordinated energy-control strategies, delay-constrained resource allocation, and mechanisms to ensure reliability under stringent delay requirements.

A. UAV-assisted Mobile Edge Computing

In recent years, research on UAV systems supporting multi-access MEC has attracted much attention. With the advantages of their excellent carrying capacity, low deployment cost and high mobility in three-dimensional space, UAVs have become a key component of future intelligent communication networks, showing unique value in expanding network coverage and enhancing communication throughput.

Earlier studies mostly relied on OMA strategies to divide time, frequency or code resources to different users through time division multiple access (TDMA), frequency division multiple access (FDMA), etc., so as to suppress co-channel interference and ensure stable operation of the system. Liu et

al. [16] explored a multi-antenna UAV-assisted MEC network and constructed a multi-antenna UAV collaborative MEC architecture with the introduction of TDMA technology. Further, El-Emary et al. [17], Ji et al. [18] focused on minimizing the ground equipment energy consumption and system weighted energy consumption, respectively, and constructed a joint optimization model. Different from them is the work of Liu et al. [19] and Xiang et al. [20], where [19] designed a deep reinforcement learning-based framework to jointly optimize the UAV 3D trajectory and user task offloading strategy, aiming to minimize the propulsion energy consumption of rotary wing UAVs. In [20], the important performance metric of delay in MEC networks is considered, and the user device task offloading decision and UAV flight trajectory are jointly optimized for UAV-MEC scenarios to balance the system energy consumption and communication delay. Wang et al. [21] propose a joint optimization framework for region division and trajectory scheduling based on optimal transmission theory by dividing the flight domain into multiple subregions with preset hovering points. However, the hovering work performed by their UAVs greatly reduces the performance of high maneuverability of UAVs. Although these OMA schemes can guarantee the connection reliability to a certain extent, their exclusive resource allocation model also limits the spectrum utilization efficiency and system capacity.

To break through the bottleneck of OMA, power-domain multiplexing NOMA is introduced into UAV-MEC networks to further improve spectrum efficiency and system throughput. To enhance UAV-MEC performance and spectrum utilization, NOMA techniques were explored in [22]–[27]: Zhang et al. [22] proposed a multi-UAV collaborative NOMA-MEC framework, minimizing weighted energy consumption via power-domain multiplexing and dynamic scheduling in a multi-UAV setup. Lu et al. [23] focused on real-time service capability for NOMA-MEC in mobile scenarios, jointly optimizing UAV trajectories with computation and communication resources to boost real-time performance. More complex hybrid non-orthogonal multiple access (H-NOMA) designs and dual UAV-NOMA architectures were also proposed to meet large-scale terrestrial device coverage and service needs [24]–[27]. Among them, Kota et al. [24] developed a H-NOMA UAV-assisted MEC framework to optimize offloading energy requirements, while Liu et al. [25] enabled UAVs to act as both mobile computation units and relays for air-ground cooperative networks serving massive users. Liu et al. [26] further proposed a dual UAV-NOMA architecture to provide coverage and compute-communication services for terrestrial IoT nodes, and He et al. [27] jointly optimized offloading decisions and 3D trajectories in multi-UAV environments with inter-UAV fairness.

These NOMA-UAV-MEC studies show that NOMA's power-domain multiplexing effectively boosts spectrum efficiency, optimized for energy consumption [22], real-time capability [23], and large-scale coverage via advanced architectures [**?**]; joint optimization of UAV trajectories, resources, and offloading is key for mobile scenario adaptability [23], [27]. However, theoretical models often ignore real-world factors (e.g., UAV range, dynamic channels, sudden mission load changes) that impact system performance.

Meanwhile, the deep integration of WPT technology with UAV-MEC has emerged as a key focus for addressing range bottlenecks. Studies have explored integrating RF-WPT or Backscatter communication to reduce user device energy consumption via parallel wireless power supply and computation scheduling [28], [29]. For example, Du et al. [28] used UAV-based RF-WPT to minimize UAV energy use while charging ground users, and Li et al. [29] combined Backscatter with RF-WPT to create a hybrid active-passive offloading framework for low-energy system operation. While these works demonstrate how wireless power integration can cut user device energy costs, they tend to center solely on ground user equipment, overlooking the system's broader energy constraints, particularly for UAVs themselves. Additionally, RF-WPT's limited distance efficiency means energy harvesting often fails to meet equipment demands.

In addition to access and energy optimization, factors like security, reconfigurability, and diverse performance metrics have driven UAV-MEC architecture innovation. For example, Gao et al. [30] and Lu et al. [31] constructed a security system model with joint trajectory and anti-eavesdropping mechanisms to maximize the security throughput and computational bits in maritime and in-flight eavesdropping scenarios, respectively. Qin et al. [32] deployed the Reflective Intelligent Surface (RIS) in the ground bypass to optimize the phase, trajectory, and computational offloading jointly to enhance the energy efficiency of the UAV-MEC system, while Tian et al. [33] improved the energy efficiency of the UAV-MEC system from the aspect of MEC performance metrics, proposed a framework for constructing a user satisfaction model based on task priority and jointly optimizing offloading and scheduling using heuristic algorithms from the aspect of MEC performance metrics. Han et al. [34] considered a heterogeneous UAV-terrestrial base stations architecture and utilized a queueing theory model to minimize the average task delay, which was achieved through user association and deployment optimization. Wang et al. [35] proposed a model-based engineering approach for improving the correctness and reliability of UAV-MEC systems in safety-critical scenarios. Together, these works highlight how multi-faceted performance goals are reshaping architecture design.

Furthermore, recent work has expanded UAV-MEC's application scenarios and methodologies. Tang et al. [36] developed a hybrid framework for UAV-supported WPCNs that merges federated learning (FL) with offloadable task processing, enabling collaborative handling of FL and non-privacy-sensitive MEC tasks in a single system. Zhou et al. [37] developed an ISAC-oriented UAV framework employing "time-assisted" beamforming and trajectory prediction. This approach estimates target states, leverages historical sensor data to optimize beamforming in real-time for subsequent time slots, and thus enhances both tracking and communication performance. These efforts show how cross-disciplinary integration (e.g., FL, ISAC) is broadening the scope of UAV-MEC research.

Existing studies have made significant strides in joint UAV trajectory and resource allocation, but they typically overlook three critical areas: closed-loop, long-term energy provisioning

for both UAVs and ground users; robust low-delay guarantees under time-varying channels and mission dynamics; and the tight coupling between WPT and NOMA with its associated impacts on transmission and energy management design. Consequently, no unified solution yet balances coverage range, delay guarantees, energy consumption, and spectral efficiency, leaving key system-level trade-offs and practical deployment challenges inadequately addressed.

B. NOMA-assisted Mobile Edge Computing

Existing OMA strategies allocate orthogonal resources such as time slots or subcarriers exclusively to different users, whereas NOMA permits multiple users to transmit simultaneously over the same time or frequency resources. Integrating NOMA into MEC systems can markedly improve spectral efficiency and overall system performance; consequently, NOMA has attracted considerable attention as a promising multiuser-access solution.

Within the NOMA–MEC literature, research has predominantly targeted two objectives: minimization of task offloading delay and improvement of energy efficiency. Irum et al. [38] and Fang et al. [39] construct multiuser NOMA–MEC network models focused on optimizing task offloading delay in coupled systems, while Huang et al. [40] explore the convergence of NOMA and MEC by proposing an uplink NOMA–based partial offloading scheme that enables multiple mobile devices to offload computation on the same time–frequency resource block, thereby enhancing fairness in both spectral and computational resource allocation. A common assumption in these studies, however, is perfect channel state information (CSI), which overlooks the impact of channel variability. To address this uncertainty, Qiu et al. [41] propose an energy–efficient allocation scheme that relies solely on statistical CSI. Separately, Li et al. [42] and Lin et al. [43] focus on performance optimization under dynamic user pairing, where [42] introduces this mechanism in MEC networks for flexible pairing across time slots, and [43] develops a systematic analytical framework for NOMA-MEC offloading incorporating practical factors like random user locations. Taken together, these studies span from approaches relying on full CSI to more practical setups that account for channel uncertainty and dynamic pairing—reflecting how research has evolved to address real-world complexities while building on insights from earlier work.

Heterogeneous NOMA–MEC architectures, distributed resource-allocation schemes, and dynamic optimization strategies have been tailored to multi-cell and multi-site deployments. Liu et al. [44] optimize energy efficiency in their heterogeneous design for multi-cellular environments, while Han et al. [45] focus on modeling and analyzing energy consumption in similar setups. Zeng et al. [46] further demonstrate that dynamic optimization can leverage NOMA's delay advantages under power and energy constraints for multi-user scenarios. Complementing these efforts, Cai et al. [47] reduce task completion time and offloading cost via distributed resource allocation in centerless multicell networks.

As NOMA–MEC research has deepened, hybrid NOMA–OMA architectures have emerged: Ding et al. [48] compare OMA and NOMA offloading in combined systems and propose a hybrid scheme, Dursun et al. [49] analyze its delay performance, Huang et al. [50] add dynamic user selection for adaptive multiple-access choices, and Ding et al. [51] formulate multi-objective optimization to minimize energy use. Yet none of these works address end-device sustainability, a key gap in hybrid network design.

To support device sustainability, WPT has been paired with NOMA–MEC: Su et al. [52] maximize computational efficiency and balance energy fairness via joint energy beamforming, time allocation, and power control in a wireless-powered system, though their model is limited to dual-user scenarios. Shi et al. [53] maximize network-level CEE with partial offloading in a WPT-based setup, but RF-WPT's high propagation loss and low long-range harvesting efficiency remain unresolved.

Other lines of work advance NOMA–MEC architecture from diverse perspectives. Liu et al. [54] employ a Taguchi Loss Function (TLF) modeling approach to quantify economic costs arising from load-tracking deviation. Zhang et al. [55] propose a hybrid NOMA-assisted MEC network-slicing scheme, grouping users and using hybrid NOMA to occupy channels so as to optimize overall network energy consumption. Du et al. [56] introduce a backscatter communication–MEC (BC-MEC) system based on NOMA to tackle low spectral utilization and limited device battery life. Yang et al. [57], focusing on the Internet of Video Things (IoVT), propose a NOMA-assisted multi-MEC IoVT system with joint optimization of packetization and offloading. Despite these advances, most of the above works assume fixed MEC servers or static user locations, and thus do not fully capture the influence of dynamic channel conditions and time-varying task arrivals on system performance.

In summary, while studies like [52]–[54] use RF-WPT to support sustainability, they overlook the inefficiency of long-distance energy harvesting for user demands. Works such as [35], [38], [56] focus on fixed MEC servers without addressing channel variability and energy-harvesting constraints together. Even those introducing dynamic user pairing (e.g., [30], [50], [57]) do not consider how MEC location changes affect inter-user channel disparities in NOMA. Additionally, [53], [56] account for energy constraints but ignore energy-causality requirements. Overall, the NOMA–MEC literature remains lacking in closed-loop long-duration energy management, robust low-delay guarantees for dynamic channels and tasks, and deep integration of high-efficiency LWPT with NOMA.

C. WPT-assisted Mobile Edge Computing

In the domain of WPT–MEC, numerous studies have advanced network architecture designs and optimization strategies from diverse perspectives, offering actionable insights through their findings. For instance, a multi-layer 3D mesh HAP–MEC system [14] demonstrated that fine-grained laser WPT coverage can safeguard the location privacy of airborne user devices, highlighting a critical balance between energy delivery and user privacy. The role of UAVs as mobile energy and computation nodes has also yielded key takeaways: works

such as [28], [29] emphasized that joint optimization of UAV hovering time, energy transfer, and offloading schedules is essential for building energy-efficient models, particularly when leveraging TDMA or hybrid active–passive communications. Liu et al. [58] further developed an air–ground cooperative framework integrating multiple UAV relays with satellite links to preserve data freshness, while Zeng et al. [59] showed that combining long- and short-term time-slot allocations with Stackelberg-game and Lyapunov-optimization techniques enables large-scale regional services via a hybrid UAV–cloud mechanism—underscoring the value of cross-strategy integration for scalability.

Convergence of heterogeneous technologies has become increasingly prominent, with lessons drawn from how different systems interact. Several studies have embedded NOMA into WPT–MEC to boost spectrum multiplexing [53], [55], [56], while Li et al. [60] and Yang et al. [61] illustrated that IRS, when combined with FDMA–NOMA protocols, can enhance channel quality and reduce delay in multi-device systems by optimizing phase-shift matrices, highlighting the impact of smart surface integration on performance metrics. Zhang et al. [62] emphasized that multidimensional resource allocation is foundational for inter-terminal cooperative computation, whereas Wang et al. [63] and Bolourian et al. [64] demonstrated that energy beamforming and cloud–MEC–device three-tier cooperation can achieve globally optimal scheduling under causal energy- and task-related constraints both in single-user scenarios and three-layer network architectures. To address integrated data-and-energy transfer (IDET) requirements, Zhang et al. [65] examined a federated-learning–assisted multi-user IDET system, revealing that this approach can jointly improve wireless data transfer (WDT) and wireless energy transfer (WET) performance in WPT–MEC networks, underscoring the potential of machine learning to enhance integrated systems.

Sustainability of device operation has also been explored, with Zhu et al. [66] and Han et al. [67] studying networked WPT–MEC solutions aimed at prolonging device operating time. Notwithstanding these advances, the literature remains dominated by RF–WPT due to consistent operational patterns in deployment, while investigations of LWPT are still nascent. Works such as [28], [29] adopt RF energy harvesting in UAV–IoT settings with TDMA/hybrid communication, and [53], [55], [56] combine RF–WPT with NOMA, backscatter, or network slicing to optimize energy consumption or efficiency—highlighting RF's role as a baseline for energy management. Similarly, [60], [61] deploy RF–WPT with IRS to improve delay and energy metrics, and [59], [62]–[64] offer in-depth treatments of RF–WPT collection, beamforming, and resource scheduling from UAV–cloud collaboration, terminal cooperation, and three-tier architecture viewpoints. Collectively, these studies have substantially contributed to topology design and protocol innovation; however, they have largely overlooked key advantages of LWPT, including its high directionality, long-range energy delivery capability, and spectral bypassing, and thus have not validated its potential to enhance coverage efficiency. This gap, rooted in the underutilization of LWPT's unique benefits, motivates further investigation into LWPT–MEC architectures and cross-layer collaborative optimization for dynamic, multi-node scenarios.

D. Summary

Table I provides a qualitative comparison with the work in this paper in terms of MEC types, multiple access techniques, UAV sustained operation, user sustained operation, optimization objectives, whether or not to form a communication-computation-supply closed loop, and WPT techniques.

Remark 1: The symbol "$\surd$" indicates that the technology or indicator was considered and used in the work, while the symbol "$\times$" indicates that the technology or indicator was not considered in the work. H-NOMA in the table denotes mixed NOMA

Current research has yet to fully explore aspects such as latency assurance, energy sustainability, mobility coupling, and interference. Specifically: (1) Existing studies predominantly optimize drone trajectories, computational offloading, and power control separately. In practical applications, these parameters are tightly coupled, necessitating a unified optimization framework that jointly addresses the coupling of energy, latency, and trajectory; (2) Although WPT technology has been introduced to extend device runtime, existing literature primarily relies on RF-WPT, which suffers from limited transmission range and low energy harvesting efficiency over long distances. Integrating efficient LWPT with adaptive energy scheduling mechanisms is crucial for achieving long-term closed-loop system sustainability that simultaneously supports ground equipment and UAVs; (3) Most models assume static or quasi-static channel conditions and stable task arrivals, failing to capture the time-varying characteristics observed in real-world deployments; (4) While numerous studies focus on improving average latency or energy efficiency, few solutions provide the stringent latency or reliability guarantees required for mission-critical and emergency applications; (5) Existing research shows limited applicability in scenarios such as natural disaster recovery and emergency response, environmental monitoring in remote areas, and high-density surveillance. To address this, we propose an LWPT-NOMA-MEC framework that achieves joint trajectory-task offloading optimization, interference suppression, and synchronous transmission of energy and data, resolving the mobile-interference-power dynamics in real-time disaster response. This framework can be better applied to the aforementioned scenarios.

The proposed network architecture can be extended to multi-UAV collaborative systems. Building upon the existing modules of task offloading, resource allocation, and trajectory optimization, the architecture can incorporate user-UAV association optimization strategies, clearly define feasible domains for resource allocation and flight safety, adopt hierarchical scheduling architectures with computationally powerful aerial nodes handling global scheduling and resource management, introduce cooperative game-based distributed optimization algorithms for fair allocation of computation and energy resources, and employ time-slot multiplexing and interference alignment techniques to mitigate communication interference, thereby enabling effective extension to multi-UAV architectures.

TABLE I
QUALITATIVE COMPARISON OF THE CURRENT LITERATURE

Reference	MEC	Multiple Access Technology	UAV Energy Supply	User Energy Supply	UAV Trajectory	Power Control	User Scheduling	Offloading Strategy	Optimization Objectives
[12]	×	×	LWPT	×	×	√	×	×	Energy Efficiency
[14]	UAV	OMA	LWPT	×	×	×	×	×	Privacy Performance
[16]	UAV	OMA	×	×	√	√	×	×	Energy Consumption
[17]	×	OMA	×	×	√	×	×	√	Energy Consumption
[18]	UAV	NOMA	×	×	√	×	×	√	Energy Consumption
[19]	UAV	OMA	×	×	√	×	×	√	Energy Efficiency
[21]	UAV	OMA	×	×	√	×	×	√	Energy Consumption
[22]	UAV	NOMA	×	×	√	√	×	×	Energy Consumption
[24]	UAV	H-NOMA	×	×	×	×	×	×	Energy Consumption
[25]	UAV	NOMA	×	×	√	√	√	×	Energy Efficiency
[26]	UAV	NOMA	×	×	√	√	√	×	Energy Efficiency
[27]	UAV	OMA	×	×	√	×	√	√	Energy Consumption
[28]	UAV	OMA	×	RF-WPT	×	×	√	×	Energy Consumption
[29]	UAV	OMA	×	RF-WPT	√	√	×	×	Computing Bite-size
[30]	×	NOMA	×	×	×	√	×	×	Secure Computing Bits
[31]	UAV	NOMA	×	×	√	√	×	×	Secure Computing Bits
[32]	UAV	NOMA	×	×	√	√	×	√	Energy Efficiency
[34]	UAV	OMA	×	×	×	×	√	×	Delay
[35]	UAV	OMA	×	×	×	×	×	×	Energy Consumption Delay
[36]	UAV	OMA	×	RF-WPT	×	√	√	√	Energy Consumption
[37]	UAV	OMA	×	×	√	√	×	×	Transmission rate
[38]	×	NOMA	×	×	×	√	×	×	Delay
[39]	×	NOMA	×	×	×	√	×	√	Delay
[40]	×	NOMA	×	×	×	√	×	×	Energy Efficiency
[41]	×	NOMA	×	×	×	√	×	×	Energy Efficiency
[42]	×	NOMA	×	×	×	√	√	√	Energy Consumption
[43]	×	NOMA	×	×	×	×	×	√	Energy Consumption Delay
[44]	×	NOMA	×	×	×	√	×	×	Energy Efficiency
[45]	×	NOMA	×	×	×	√	×	×	Energy Efficiency
[46]	×	NOMA	×	×	×	√	×	×	Delay
[47]	×	NOMA	×	×	×	√	×	√	costs
[48]	×	NOMA	×	×	×	√	×	×	Energy Consumption
[49]	×	H-NOMA	×	×	×	√	×	×	Delay
[50]	×	H-NOMA	×	×	×	√	×	×	Energy Consumption
[51]	×	H-NOMA	×	×	×	√	×	×	Energy Consumption
[52]	×	NOMA	×	×	×	√	×	√	Energy Consumption
[53]	×	NOMA	×	RF-WPT	×	√	×	×	Energy Efficiency
[54]	×	NOMA	×	×	×	√	×	√	Energy Consumption
[55]	×	H-NOMA	×	RF-WPT	×	√	×	√	Energy Consumption
[56]	×	NOMA	×	RF-WPT	×	√	×	×	Energy Efficiency
[57]	×	NOMA	×	×	×	×	×	√	Energy Consumption Delay
[58]	UAV	OMA	×	RF-WPT	√	√	√	×	Average Age of Information
[59]	UAV	OMA	RF-WPT	×	√	√	×	×	Delay
[60]	×	NOMA	×	RF-WPT	×	√	×	×	Delay
[61]	×	OMA	×	RF-WPT	×	√	×	√	Energy Consumption
[62]	×	OMA	×	RF-WPT	×	√	√	√	Energy Consumption
[63]	×	OMA	×	RF-WPT	×	√	×	√	Energy Consumption
[64]	×	OMA	×	RF-WPT	×	√	×	√	Energy Consumption
[65]	×	OMA	×	RF-WPT	×	×	×	×	Energy Harvesting
[67]	×	NOMA	×	RF-WPT	×	√	√	×	Energy Efficiency
This work	UAV	NOMA	LWPT	RF-WPT	√	√	√	√	Delay

This paper focuses on constructing energy-constrained single-UAV edge computing systems for typical scenarios including emergency patrol, remote area monitoring, and environmental data collection. These applications feature limited service targets, confined geographical coverage, and relatively concentrated tasks, so a single UAV can efficiently complete data collection and computational tasks while delivering superior deployment flexibility and cost-effectiveness. Therefore, this paper first conducts in-depth analysis and validation of energy bottlenecks and access efficiency on single-UAV platforms, providing theoretical foundations and algorithmic benchmarks for subsequent extension to multi-UAV collaborative systems.

III. System Model And Problem Formulation

We investigate a UAV-assisted MEC network system consisting of a UAV equipped with a MEC server and an energy transmitter, $M(M \geq 1)$ uniformly distributed users, and a laser PB, where both the UAV and ground user devices are equipped with rechargeable batteries. Users are required to complete tasks by time T. Due to limited device computing power, the UAV provides enhanced computational services.

TABLE II
NOTATION TABLE

Symbol	Description
M	Number of users
B	Channel bandwidth
T	System cycle duration
τ	Time slot cycle time
N	Number of time slots
V_{max}^{uav}	Maximum flight speed of the UAV
S	Number of internet users
λ_m	User uninstallation rate
α_m	User scheduling policy
h_K	Channel gain between the user and the UAV
D_K	User calculates task size
ε_K^{user}	Effective switching capacitance of the user
f_K^{user}	User CPU calculation frequency
C_K^{user}	The user CPU computes 1-bit data cycles
ε^{uav}	Effective switching capacitance of the UAV
f_K^{uav}	UAV CPU calculation frequency
C^{uav}	The UAV CPU computes 1-bit data cycles
P_K	User transmit power
P_b	Laser PB transmit power
β	UAV energy conversion factor
A	Receiving lens area
d_b	Distance between UAV and PB
D	Size of the emitted laser beam
$\triangle\theta$	Angular spreading degree
χ	Receiver optical efficiency
α_1	Attenuation factor

Advanced wireless communication enables efficient data transfer between the UAV and users, with NOMA technology supporting concurrent communication, reducing delay, and improving spectral efficiency.

To mitigate the UAV's onboard energy constraints, the system integrates two key modules on the airframe: an energy-harvesting circuit (for UAV self-powering) and an energy-transmission module (for user power delivery). First, a laser PB provides continuous energy to the UAV via LWPT. An onboard photovoltaic (PV) receiver along with a power management circuit converts the harvested optical energy into electrical power, sustaining the UAV's propulsion system and computing payload. In addition, the UAV is equipped with an RF-WPT transmitter and a directional antenna array that emits a focused RF beam toward ground users. Each user employs a compact rectenna module to harvest this RF energy, enabling wireless power supply to their terminal devices. Fig. 1 illustrates the system model, highlighting key components and interactions. Some important notations are summarized in Table II.

We define the set $\mathcal{M} = \{1, \ldots, M\}$ to index users in the system. A three-dimensional Cartesian coordinate system is employed to specify the positions of the users, the UAV, and the laser PB. The coordinates of user $m \in \mathcal{M}$ and the PB are represented as $\mathbf{Q}_m^{user} = (x_m^{user}, y_m^{user}, 0)$ and $\mathbf{Q}^b = (x^b, y^b, h^b)$, respectively. To tackle the UAV trajectory optimization problem, we utilize a path discretization method. The UAV's continuous trajectory is divided into $N(N > 1)$ discrete segments, with each segment connecting consecutive points. Thus, the continuous flight path is approximated by a series of linear segments. Although the entire calculation process is continuous in time, the interval can be discretized into N time slots of equal length τ. The set $\mathcal{N} = \{1, \ldots, N\}$ denotes these discrete time slots. During each time slot $n \in \mathcal{N}$, the UAV's position is updated, denoted as $\mathbf{Q}^{uav}[\mathrm{n}] = (x^{uav}[\mathrm{n}], y^{uav}[\mathrm{n}], h^{uav})$. Assuming the UAV maintains a constant altitude throughout its flight, with only its horizontal coordinates changing, it completes a circular trajectory and returns to its starting position after a cycle time T, following as:

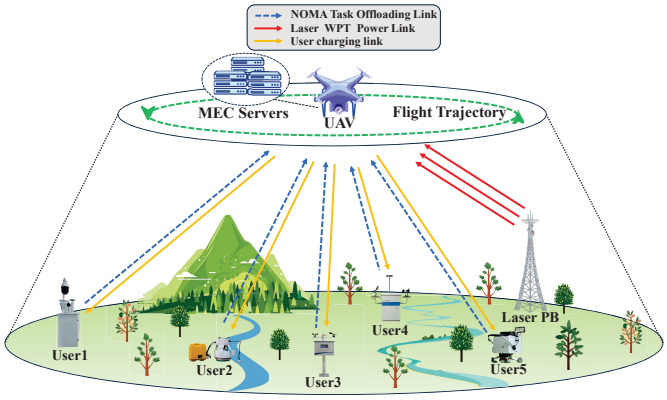

Fig. 1. Schematic diagram of the proposed network model.

$$\mathbf{Q}^{uav}[1] = \mathbf{Q}^{uav}[N]. \tag{1}$$

If the UAV moves uniformly within each time slot and its speed remains below the maximum permissible limit, the following constraint must be satisfied:

$$\frac{\|\mathbf{Q}^{uav}[n] - \mathbf{Q}^{uav}[n-1]\|}{\tau} \leq V_{\max}^{uav}. \tag{2}$$

Throughout this study, the UAV maintains a constant flight altitude [68]. Consequently, the distance between the UAV and user m during the n^{th} time slot is given by:

$$d_m[n] = \sqrt{(x^{uav}[n] - x_m^{user})^2 + (y^{uav}[n] - y_m^{user})^2 + (h^{uav})^2}. \tag{3}$$

Similarly, the distance between the UAV and the laser PB during the n^{th} time slot is denoted by:

$$d_b[n] = \sqrt{(x^{uav}[n] - x^b)^2 + (y^{uav}[n] - y^b)^2 + (h^{uav} - h^b)^2}. \tag{4}$$

A. User Scheduling Model

Due to the limitations of UAV communication and computing resources, the system allows S users to communicate with the UAV in each time slot [69], [70]. To represent this, we introduce a binary variable $\alpha_m[n] \in \{0, 1\}$, where $\alpha_m[n] = 1$ signifies that the UAV schedules a connection with user m during time slot n, thereby allowing the user to access the uplink NOMA network. Conversely, $\alpha_m[n] = 0$ indicates that the UAV does not communicate with the user during that time slot. The user scheduling policy can thus be expressed as follows:

$$\alpha_m[n] \in \{0, 1\}, \tag{5}$$

$$\sum_{m \in \mathcal{M}} \alpha_m[n] = S. \tag{6}$$

In the proposed scheme, the number of users S that can communicate with the UAV in each time slot is significantly smaller than the total number of users M in the system, $S << M$. Consequently, during each n^{th} time slot, the UAV prioritizes communication with the S users who are closest to it, providing them with services. To represent this approach, we define an access matrix for all the time slots.

$$\mathbf{K} = (K_i^n)_{S\times N} = \begin{bmatrix} K_1^1 & K_1^2 & \cdots & K_1^N \\ K_2^1 & K_2^2 & \cdots & K_2^N \\ \cdots & \cdots & \cdots & \cdots \\ K_S^1 & K_S^2 & \cdots & K_S^N \end{bmatrix}. \quad (7)$$

Each n^{th} column in this matrix denotes the group of users who can communicate with the UAV during the n^{th} time slot, represented as $\mathcal{K}^n = \{K_1^n, K_2^n, \ldots, K_S^n\}^T \in \mathcal{M}$. These users are prioritized based on their channel conditions with the UAV to ensure effective communication between users and UAV. The priority of accessible users is as follows:

$$d_{u,K_1^n}[n] \geq d_{u,K_2^n}[n] \geq \cdots \geq d_{u,K_S^n}[n]. \quad (8)$$

Consequently, the UAV grants access to the NOMA network for these selected users, adhering to the established criteria set forth in equation (7).

B. Channel Model

For the communication channel, we use the probabilistic path loss model in [69], [71], where the average channel gain between the UAV and user K_i^{th} in the n^{th} time slot can be expressed as:

$$\overline{h}_{K_i^n}[n] = \Phi^{LoS}\frac{\sqrt{\alpha_0^{LoS}}}{d_{K_i^n}[n]^{\alpha_1{}^{LoS}}} + (1-\Phi^{LoS})\frac{\sqrt{\alpha_0^{NLoS}}}{d_{K_i^n}[n]^{\alpha_1{}^{NLoS}}}, \quad (9)$$

where Φ^{LoS} is the probability of LoS between user and the UAV, α_0^{LoS} and α_0^{NLoS} are the reference channel gains at 1m distance for the LoS and Non-Line-of-Sight (NLoS) channels, respectively, and $\alpha_1{}^{LoS}$ and $\alpha_1{}^{NLoS}$ are the path loss exponents. Following [69], [71], the probability of LoS is given by

$$\Phi^{LoS} = \frac{1}{1+\rho_2 \exp\left\{-\rho_1\left[\frac{180}{\pi}\arcsin(\frac{h^{uav}}{d_{K_i^n}[n]}) - \rho_2\right]\right\}}, \quad (10)$$

where $\frac{180}{\pi}\arcsin(\frac{h^{uav}}{d_{K_i^n}[n]})$ is the elevation angle, ρ_1 and ρ_2 are two constant values that depend on the environment.

Following arguments in [72], we assume that the UAV maintains a sufficiently high altitude throughout the system cycle and that the average channel gain between the UAV and the ground user is dominated by the LoS term. It is also assumed that the Doppler effect due to UAV maneuvering is well compensated. The channel gain between the UAV and the K_i^{th} user at the n^{th} time slot can be approximated as:

$$\overline{h}_{K_i^n}[n] \approx \Phi^{LoS}\frac{\sqrt{\alpha_0^{LoS}}}{d_{K_i^n}[n]^{\alpha_1{}^{LoS}}} = h_{K_i^n}[n]. \quad (11)$$

In typical scenarios such as disaster area inspections, environmental monitoring, and infrastructure inspections, ground nodes are typically distributed within a fan-shaped area with a known radius and relatively concentrated distribution. When a UAV patrols this area at a fixed altitude h^{uav}, the straight-line distance to each node changes only slightly, and the differences in their horizontal projections are small, resulting in minimal fluctuations in elevation angle [72]. Therefore, the UAV's inflection point elevation angle ρ_2 typically falls within a fixed range, allowing the actual elevation angle between the UAV and ground nodes to be approximated as equivalent to this inflection point angle ρ_2.

In each time slot, the UAV employs SIC to mitigate multiple access interference by utilizing different signal power levels to decode messages from various users. In uplink NOMA, signals from users with higher channel gains are decoded first [70]. Therefore, the SIC decoding sequence follows the descending order of the users' current channel gains. When the UAV's server decodes the signal from user K_s^n, the transmissions from users K_1^n to K_{s-1}^n are treated as interference. Once the signal from user K_s^n is successfully decoded, it is subtracted from the superimposed signal. The server then proceeds to decode the signal from user K_{s-1}^n, and the iterative process continues until the signal from user K_1^n is decoded. By the time the server decodes the signal from user K_1^n, there is no further interference. Therefore, in the n^{th} time slot, the signal-to-interference-plus-noise ratio (SINR) of the signal received by the UAV from user $K_i^n (1 \leq i \leq S)$ is given by:

$$\gamma_{K_i^n}[n] = \frac{P_{K_i^n}[n]\|h_{K_i^n}[n]\|^2}{\sum_{j=1}^{i-1} P_{K_j^n}[n]\|h_{K_j^n}[n]\|^2 + \sigma^2}. \quad (12)$$

The achievable transmission rate from user K_i^n to the UAV in the n^{th} time slot is expressed by:

$$R_{K_i^n}[n] = B\log_2\left(1+\gamma_{K_i^n}[n]\right), i \in \mathcal{S} = \{1,2,...,S\}, \quad (13)$$

where B means the channel bandwidth.

Remark 1: In the proposed scheme, the number of users S that can access the UAV in each time slot is generally much smaller than the total number of terrestrial devices M. This disparity increases the likelihood of establishing LoS links. Furthermore, by maintaining $S \leq K$, we mitigate error accumulation and reduce the complexity associated with SIC, thereby enhancing the practicality and efficiency of the system [69].

C. Task Computation Model

In this paper, we assume that the users also possess a certain level of computational capability. Therefore, we adopt a partial offloading strategy, represented by the variable $\lambda_m[n]$ for $n \in \mathcal{N}$ and $m \in \mathcal{M}$, to denote the offloading decision of the m^{th} user in the n^{th} time slot. The variable $\boldsymbol{\lambda}$ must satisfy the following constraints:

$$0 \leq \boldsymbol{\lambda} \leq 1. \quad (14)$$

Let $D_m[n]$ represent the computational task of the m^{th} user in the n^{th} time slot. This task is divided into two segments: local computation and UAV edge computation.

1) *Local Computation:* In this scenario, the task is processed locally by the ground user. The fraction of the task executed locally by the K_i^n user in the n^{th} time slot is given by:

$$(1-\lambda_{K_i^n}[n])D_{K_i^n}[n], \tag{15}$$

the power consumption of the CPU in user K_i^n is modeled as $\kappa_{K_i^n}^{user}\left(f_{K_i^n}^{user}\right)^3$, where $\kappa_{K_i^n}^{user}$ represents the effective switching capacitance, and $f_{K_i^n}^{user}$ means the computational frequency of the CPU. The execution time for local computation is expressed as:

$$T_{c,K_i^n}^{user}[n]=\frac{(1-\lambda_{K_i^n}[n])D_{K_i^n}[n]C_{K_i^n}^{user}}{f_{K_i^n}^{user}}, \tag{16}$$

here, $C_{K_i^n}^{user}$ indicates the number of CPU cycles required to complete a 1-bit computation task. The subscript c in $T_c^{user}[n]$ denotes computation, i.e., T_c denotes computation delay and E_c denotes computation energy consumption. The subscript t in the following denotes transmission, i.e., T_t is the transmission delay and E_t is the transmission energy consumption. The energy consumption for local computation is given by [18]:

$$E_{c,K_i^n}^{user}[n]=\kappa_{K_i^n}^{user}(1-\lambda_{K_i^n}[n])D_{K_i^n}[n]C_{K_i^n}^{user}(f_{K_i^n}^{user})^2. \tag{17}$$

2) *UAV Edge Computation:* When offloading tasks to the UAV, the delay and energy consumption for the K_i^n user in the n^{th} time slot are described by:

$$T_{t,K_i^n}^{user}[n]=\frac{\lambda_{K_i^n}[n]D_{K_i^n}[n]}{R_{K_i^n}[n]}, \tag{18}$$

and

$$E_{t,K_i^n}^{user}[n]=\frac{P_{K_i^n}[n]\lambda_{K_i^n}[n]D_{K_i^n}[n]}{R_{K_i^n}[n]}, \tag{19}$$

the execution time for the task offloaded to the UAV edge server is:

$$T_{c,K_i^n}^{uav}[n]=\frac{\lambda_{K_i^n}[n]D_{K_i^n}[n]C^{uav}}{f_{K_i^n}^{uav}}, \tag{20}$$

where C^{uav} represents the number of CPU cycles needed by the UAV server to complete a one-bit task, and $f_{K_i^n}^{uav}$ is the CPU frequency allocated for user K_i^n. The energy consumption of the UAV's edge computing CPU is given by:

$$E_{c,K_i^n}^{uav}[n]=\kappa^{uav}\lambda_{K_i^n}[n]D_{K_i^n}[n]C^{uav}(f_{K_i^n}^{uav})^2, \tag{21}$$

where κ^{uav} denotes the effective switching capacitance of the UAV's CPU.

D. UAV Flight Energy Consumption Model

The energy consumption of a UAV during flight is determined by its speed and flight duration. The energy model for the UAV in each time slot is described as follows [13]:

$$E^{fly}[n]=\eta\frac{W^{uav}\tau}{2}(\frac{\|\mathbf{Q}^{uav}[n]-\mathbf{Q}^{uav}[n-1]\|}{\tau})^2, \tag{22}$$

here, η represents the UAV's flight energy consumption coefficient, and W^{uav} denotes the weight of the UAV.

E. Energy Harvesting Model

To facilitate extended remote operation, the UAV platform is equipped with an energy-harvesting circuit that enables efficient power collection from a laser PB during both flight and mission execution. Compared with microwave or radio-frequency transfer, laser transmission features a much smaller beam divergence angle, allowing highly directional energy delivery over distances ranging from several hundred meters to kilometers; this markedly reduces power loss and thereby prolongs UAV endurance, satisfying the requirements for sustained flight in emergency or remote environments. Although laser propagation is susceptible to atmospheric visibility fluctuations, fog, and precipitation, meteorological conditions in most emergency-response or post-disaster reconstruction scenarios can be forecasted or monitored in real time. By integrating live weather monitoring with predictive scheduling, laser charging can be conducted during high-visibility intervals, storing the harvested energy in the UAV's battery to ensure continuous operation. To guarantee the safety of personnel and equipment, this study employs an eye-safe laser source that conforms to established safety standards, tightly regulates irradiance levels, and incorporates a rapid beam-shutting mechanism. These measures collectively limit environmental and safety risks to acceptable levels, thereby providing safety assurance in dynamic, remote, or unpredictable mission environments.

It is assumed that when the UAV is being charged using LWPT, the UAV remains relatively stationary with respect to the laser PB. The energy harvesting model for each time slot is given by [15]:

$$E_{eh}[n]=\beta\tau\frac{P_b[n]A\chi e^{-\alpha_1 d_{as}[n]}}{\left(D+d_{as}[n]\Delta\theta\right)^2}, \tag{23}$$

where $\beta\in(0,1)$ is the energy conversion factor, $P_b[n]$ is the transmit power of the PB, A is the area of the receiver telescope or collection lens, D is the size of the initial laser beam, $\Delta\theta$ is the angular spread, χ is the combined transmission receiver optical efficiency, and α_1 is the attenuation coefficient of the medium.

As the UAV's flight altitude increases, it gradually moves away from densely populated areas with ground structures and trees. When the flight altitude reaches a certain height, the impact of physical obstacles on the communication link will be significantly reduced, and the LoS channel becomes the dominant path for wireless transmission. Therefore, during the drone's cruise flight, the probability of communication link interruptions or NLoS conditions occurring is significantly reduced, facilitating a reliable LoS connection with the laser PB. To further ensure the continuity of LWPT, the drone is equipped with rechargeable energy storage batteries that provide energy buffering when the laser power source is temporarily interrupted, thereby enhancing the system's robustness and operational stability.

Given the short duration of each scheduling time slot and the UAV's limited flight speed, the relative position and link geometry between the UAV and each user remain approximately constant within a slot, resulting in negligible fluctuations in

the free-space channel gain. To account for minor path loss variations, the UAV's onboard power management circuitry dynamically adjusts the transmit power in real time. To balance model simplicity with accuracy, we adopt a linear energy harvesting model for user i in time slot n, approximated as:

$$E_{eh,i}^{user}[n] = \eta_i \, P_u \, h_{u,i}[n] \, \tau \approx E_{eh}^{K_i^n}[n], \tag{24}$$

where η_i represents the energy-conversion efficiency of user i, P_u is the UAV's RF transmit power in time slot n, $h_{u,j}[n]$ is the channel gain between the UAV and user i, and τ is the duration of the time slot.

F. Problem Formulation

Based on the previously described LWPT uplink NOMA UAV-assisted MEC system model, we now formulate the corresponding optimization problem. It is assumed that the UAV is capable of performing task computation while simultaneously receiving tasks, and users commence local computation immediately after offloading. The system delay composition for each time slot is: the combined offloading time and the user's local computation execution time $T_{t,K_i^n}^{user}[n] + T_{c,K_i^n}^{user}[n]$, and the UAV's edge computation execution time $T_{c,K_i^n}^{uav}[n]$. The UAV transmits the computation results back to the user within the same time slot. Given the relatively small size of the computation results compared to the offloaded task data, the time and energy required for sending the results back to the user are considered negligible [73], [74]. The primary objective of this paper is to minimize the time delay for the UAV to serve users in each time slot over T time periods by jointly optimizing the offloading task ratio $\boldsymbol{\lambda}$, the user scheduling variable $\boldsymbol{\alpha}$, the PB transmit power $\mathbf{P}_b$, and the UAV's flight trajectory $\boldsymbol{Q}^{uav}$. The optimization problem is formulated as follows:

$$\begin{aligned}
\mathbf{P1}: & \min_{\boldsymbol{\lambda},\boldsymbol{\alpha},\mathbf{P}_b,\boldsymbol{Q}^{uav}} \sum_{n=1}^{N} \max_{K_i^n \in \mathbf{K}} \{T_{t,K_i^n}^{user}[n] + T_{c,K_i^n}^{user}[n], T_{c,K_i^n}^{uav}[n]\} \\
s.t. & C1: \sum_{i=1}^{M} \alpha_{K_i^n}[n] = S, K_i^n \in \mathcal{K}^n, n \in \mathcal{N}, \\
& C2: \alpha_{K_i^n}[n] \in \{0,1\}, K_i^n \in \mathcal{K}^n, n \in \mathcal{N}, \\
& C3: 0 \le \lambda_{K_i^n}[n] \le 1, K_i^n \in \mathcal{K}^n, n \in \mathcal{N}, \\
& C4: 0 \le P_b[n] \le P_b^{\max}, n \in \mathcal{N}, \\
& C5: \mathbf{Q}^{uav}[1] = \mathbf{Q}^{uav}[N], \\
& C6: \frac{\|\mathbf{Q}^{uav}[n] - \mathbf{Q}^{uav}[n-1]\|}{\tau} \le V_{\max}^{uav}, n \in \mathcal{N}, \\
& C7: E^{fly}[n] + E_{c,K_i^n}^{uav}[n] \le \\
& \qquad E_0^{uav} + E_{eh}[n], K_i^n \in \mathcal{K}^n, n \in \mathcal{N}, \\
& C8: E_{c,K_i^n}^{user}[n] + E_{t,K_i^n}^{user}[n] \le \\
& \qquad E_0^{K_i^n} + E_{eh}^{K_i^n}[n], K_i^n \in \mathcal{K}^n, n \in \mathcal{N}.
\end{aligned} \tag{25}$$

$\mathbf{K}$ is an $S \times N$ matrix, where each element represents a user-accessible during the cycle, and each column vector indicates the sequence of SIC that changes in each time slot. Where constraints $C1$ and $C2$ limit the number of users that can access the uplink NOMA network to S users per time slot. $C3$ ensures that the offloading rate for each user remains within the range $[0, 1]$ in each time slot. $C4$ imposes a restriction on the PB, with $P_b^{\max}$ indicating the maximum transmission power. $C5$ governs the UAV's flight trajectory. $C6$ imposes a limit on the UAV's flight speed, ensuring it does not surpass the maximum speed in any time slot. In each time slot, UAVs and users can continuously recharge their batteries through laser or radio frequency wireless energy transfer during flight or mission execution. Constraints $C7$ and $C8$ are based on the principle of energy causality, incorporating the initial battery energy and the energy collected in sequence into the constraints to ensure that the cumulative energy consumption in any time slot does not exceed the sum of the initial stock and the energy already collected. $E_0^{K_i^n}$ and E_0^{uav} are the initial battery energies of the user and the UAV, respectively.

IV. Joint Alternating Optimization Algorithm for Trajectory and Resource Allocation

The presence of binary variables in the problem (25) turns it into a mixed-integer programming (MIP) problem. To address this challenge, we present an efficient user scheduling strategy to determine which users access the uplink NOMA network in each time slot.

In practical applications such as disaster monitoring, environmental sensing, and infrastructure inspection, ground users are typically stationary or exhibit very limited mobility. Examples include fixed-location sensors, temporary rescue stations, or low-speed mobile base station equipment, whose positions remain largely unchanged throughout the task execution period. In contrast, UAVs have high maneuverability and can quickly move to designated locations according to task requirements. In our trajectory-optimization framework, we employ a path-discretization approach combined with a stepwise optimization strategy. At each waypoint, the UAV first selects the S users with the highest channel gains at its current position; since ground users' locations do not change, these same S users continue to enjoy strong link quality and can be regarded as the optimal access candidates. Crucially, as the UAV moves to the next waypoint, the system recalculates every user's channel gain based on the updated trajectory and then reselects the top S users. By alternately updating trajectory and user-association decisions, this process ensures that user selection dynamically tracks the UAV's instantaneous position, thereby improving overall system performance.

Since this scheduling strategy is closely related to the initial UAV trajectory, to ensure maximum fairness, the initial UAV trajectory should cover all ground users so that all users have the opportunity to access the uplink NOMA network from the start. The details are summarized in Algorithm 1.

Algorithm 1 Trajectory-Aware User Scheduling Strategy

Initialization:
  Determine the number of accessible users S
  Initialize the access matrix $\mathbf{K}$
  Design UAV flight trajectory $\boldsymbol{Q}^{uav}$ to ensure coverage of all ground users
  Set time slot $n = 1$
Repeat
  Measure the instantaneous channel gains for each currently covered user at the current UAV position via (11).
  Obtain optimal access group $\mathcal{K}^{n*}$ based on current channel conditions and UAV trajectory for temporal fairness.
  Set user scheduling $\{\alpha_l[n] = 1, l \in \mathcal{K}^{n*}\}$, $\alpha_l[n] = 0$ when $l \notin \mathcal{K}^{n*}$
  $n = n + 1$
Until The maximum number of time slots N is satisfied
Output: $\mathbf{K}^* = \{\mathcal{K}^{1*}, \mathcal{K}^{2*}, \ldots, \mathcal{K}^{N*}\}^T$

In Algorithm 1, the user scheduling strategy is based on instantaneous channel gain, with the core objective of maximizing system throughput to minimize total task offloading delay. The effectiveness of this strategy in the initial phase is closely tied to the UAV's initial flight trajectory. To ensure fairness during access, we incorporate an initial trajectory in the system design that covers all ground users, enabling every user to access the NOMA uplink at the start of service and initiate initial task offloading.

As the UAV moves throughout task execution, the relative positions between users and the UAV change continuously, leading to dynamic channel fluctuations. Even with scheduling based on instantaneous channel gains, users can experience channel-advantaged states in different time slots, so they still receive scheduling opportunities. This scheduling strategy comprehensively considers the energy and time constraints of the UAV-assisted MEC system. Under limited UAV energy and service windows constraints, prioritizing users with good channel conditions helps improve task processing efficiency per unit of energy consumption, thereby maximizing the system's overall computational performance. While ensuring users' basic access opportunities, this strategy achieves a reasonable balance between user access fairness and resource utilization efficiency, ultimately better achieving the core performance goal of system delay optimization.

Algorithm 1 employs a user scheduling algorithm that operates in an online manner. In each time slot, when the UAV arrives at its current position along the predetermined trajectory, it obtains the instantaneous channel gains of ground users within its current coverage area. The scheduling decision for that time slot is based on these locally observed channel conditions, as well as trajectory progression and fairness requirements, without relying on any future or global channel state information.

In Algorithm 1, the access matrix $\mathbf{K}$ is directly influenced by the UAV trajectory $\boldsymbol{Q}^{uav}$, which indicates $\mathbf{K}$ changes as $\boldsymbol{Q}^{uav}$ changes. By using Algorithm 1, we can determine the optimal $\mathbf{K}$ for a given trajectory $\boldsymbol{Q}^{uav}$. Thus, the optimization problem in (25) can be simplified to:

$$\begin{aligned} \mathbf{P2}: & \min_{\boldsymbol{\lambda}, \mathbf{P}_{as}, \boldsymbol{Q}^{uav}} \sum_{n=1}^{N} \max_{K_i^n \in \boldsymbol{K}^*} \{T_{t,K_i^n}^{user}[n] + T_{c,K_i^n}^{user}[n], T_{c,K_i^n}^{uav}[n]\} \\ & s.t. \quad C1^*: K_i^n \in \boldsymbol{K}^*, i \in \mathcal{S}, n \in N, \\ & \quad C3, C4, C5, C6, C7, C8. \end{aligned} \tag{26}$$

The proposed user scheduling strategy simplifies the original problem, reducing its complexity. However, the optimization objective function and constraints $C7$ and $C8$ in problem $\mathbf{P2}$ make it a non-convex optimization problem, which is a recognized NP-hard challenge that is difficult to solve directly. To address this, we propose an alternating optimization algorithm based on SCA.

This approach decomposes the original problem into two tractable subproblems: one focuses on optimizing offloading decisions and transmission power while keeping the UAV trajectory fixed, and the other targets UAV trajectory scheduling with fixed offloading decisions and transmission power. We first solve each subproblem individually to obtain their optimal solutions, then iteratively alternate between the subproblems, refining the solutions step-by-step until we achieve the optimal solution for $\mathbf{P2}$.

Problem $\mathbf{P2}$ is decomposed into two sub-problems, which are relatively straightforward to handle for the purpose of solving it. The first subproblem is the optimization of the offloading ratio and PB transmit power given the UAV trajectory, defined as $\mathbf{SP3}$. The second subproblem is the optimization of the UAV trajectory scheduling given the offloading ratio and PB transmit power, defined as $\mathbf{SP4}$. By solving the two subproblems in alternating optimization, the optimal solution of the original problem can be gradually approximated. The solution process of the two subproblems is described below.

A. Sub-problem 1: Optimization of Offloading Decisions and Transmission Power

To address subproblem $\mathbf{SP3}$ with a given initial UAV trajectory, we need to determine the optimal offloading decisions and power allocation strategy. The subproblem is formulated as follows:

$$\begin{aligned} \mathbf{SP3}: & \min_{\boldsymbol{\lambda}, \mathbf{P}_{as}} \sum_{n=1}^{N} \max_{K_i^n \in \boldsymbol{K}^*} \{T_{t,K_i^n}^{user}[n] + T_{c,K_i^n}^{user}[n], T_{c,K_i^n}^{uav}[n]\} \\ & s.t. \quad C1^*, C3, C4, C7, C8. \end{aligned} \tag{27}$$

To further simplify SP3 and eliminate the impact of the max function in the objective function, we introduce a relaxation factor $\{t_{K_i^n}[n], K_i^n \in \mathbf{K}^*, i \in \mathcal{S}, n \in \mathcal{N}\}$, where $t_{K_i^n}[n] = \max_{K_i^n \in \mathbf{K}^*} \{T_{t,K_i^n}^{user}[n] + T_{c,K_i^n}^{user}[n], T_{c,K_i^n}^{uav}[n]\}$. Transforming the original problem into:

$$\begin{aligned} \mathbf{SP3}^*: & \min_{\boldsymbol{\lambda}, \mathbf{P}_{as}} \sum_{n=1}^{N} t_{K_i^n}[n] \\ & s.t. \quad C1^*, C3, C4, C7, C8, \\ & \quad C9: T_{c,K_i^n}^{uav}[n] \le t_{K_i^n}[n], n \in N, \\ & \quad C10: T_{c,K_i^n}^{user}[n] + T_{t,K_i^n}^{user}[n] \le t_{K_i^n}[n], n \in N. \end{aligned} \tag{28}$$

In $\mathbf{SP3}^*$, the UAV trajectory is fixed, which means the UAV's flight energy consumption $E^{fly}[n]$ and access matrix $\mathbf{K}^*$ are predetermined. As a result, the transmission rate for each user in each time slot is fixed, leaving the offloading ratio and PB transmit power as the only variables to be optimized. This transformation converts the objective function from a non-convex form to an affine function of $\boldsymbol{\lambda}$, thus making it convex. Additionally, constraint $C8$ changes from a non-convex constraint to an affine function of $\boldsymbol{\lambda}$ and $\mathbf{P}_b$, rendering constraints $C7$ to $C10$ convex.

Therefore, subproblem $\mathbf{SP3}^*$ becomes a convex optimization problem, solvable using standard convex optimization techniques such as interior point methods [75]. The optimal solution for $\mathbf{SP3}^*$ is found by iteratively solving the subproblem until convergence or reaching the maximum number of iterations. The solution process is outlined in Algorithm 2.

Algorithm 2 Offloading decisions and PB transmit power optimization

1: Initialize the UAV trajectory $\boldsymbol{Q}^{uav}$, the number of iterations $l=0$, and initial utility ζ_0.
2: Update $\mathbf{K}^*$ via Algorithm 1.
3: **Repeat**
4: For $\boldsymbol{Q}^{uav}$ and $\mathbf{K}^*$, solve subproblem $\mathbf{SP3}^*$ to obtain the $\zeta_{l+1} = \underset{\boldsymbol{\lambda},\mathbf{P}_b}{argmin} \sum_{n=1}^{N} t_{K_i^n}[n]$.
5: $l = l+1$.
6: **Until** Convergence or the maximum number of iterations is satisfied.
7: Output: $\boldsymbol{\lambda}$, $\mathbf{P}_b$.

B. Sub-problem 2: Optimization of UAV Trajectory Scheduling

By solving the offloading ratio $\boldsymbol{\lambda}$ and PB transmit power $\mathbf{P}_b$ from subproblem $\mathbf{SP3}^*$, we reformulate the UAV trajectory optimization problem as follows:

$$\begin{aligned} \mathbf{SP4}: \min_{\boldsymbol{Q}^{uav}} \quad & \sum_{n=1}^{N} \max_{K_i^n \in \boldsymbol{K}^*} \{T_{t,K_i^n}^{usex}[n]\} \\ s.t. \quad & C1^*, C5, C6, C7, C8. \end{aligned} \tag{29}$$

In subproblem $\mathbf{SP4}$, the decision variable is the UAV's trajectory, which directly impacts the channel gain between the users, the PB, and the UAV. Due to the non-convex nature of the objective function and constraints $C7$ and $C8$, $\mathbf{SP4}$ is a non-convex optimization problem and thus cannot be solved directly. To tackle this, we propose an approximate solution algorithm using the SCA framework.

To further simplify $\mathbf{SP4}$ and eliminate the impact of the max function in the objective, we introduce a relaxation variable $\{\tilde{t}_{K_i^n}[n], K_i^n \in \mathbf{K}^*, i \in \mathcal{S}, n \in \mathcal{N}\}$, reformulating the objective function in $\mathbf{SP4}$ as:

$$\begin{aligned} \min_{\boldsymbol{Q}^{uav}} \quad & \sum_{n=1}^{N} \tilde{t}_{K_i^n}[n] \\ s.t. \quad & C9: T_{t,K_i^n}^{user}[n] \le \tilde{t}_{K_i^n}[n]. \end{aligned} \tag{30}$$

Since constraint $C9$ remains non-convex, we further introduce slack variables $\{r_{K_i^n}[n]\}$, yielding:

$$\begin{aligned} \tilde{T}_{t,K_i^n}^{user}[n] &= \frac{\lambda_{K_i^n}[n] D_{K_i^n}[n]}{r_{K_i^n}[n]} \\ s.t. \quad & C10: r_{K_i^n}[n] \le R_{K_i^n}[n], \end{aligned} \tag{31}$$

although $\tilde{T}_{t,K_i^n}^{user}[n]$ becomes a convex function, the right-hand side of $C10$ remains complex and non-convex due to user interference. To simplify, we introduce an additional constraint [74]

$$C11: \sum_{i=1}^{S-1} P_{K_i^n}[n] \| h_{K_i^n}[n] \|^2 \le \chi_t[n]. \tag{32}$$

This constraint represents the maximum interference a user can tolerate in each time slot. While this added constraint modifies the lower bound of the problem, adjusting $\chi_t[n]$ [74] can still yield good system performance. When α_1^{LoS} is even and the LoS probability is 1, the processed $\hat{R}_{K_i^n}[n]$ is expressed as

$$\hat{R}_{K_i^n}[n] = B \log_2 \left(1 + \frac{P_{K_i^n}[n] \alpha_0^{LoS}}{(\chi_t[n] + \sigma^2) \| Q^{uav}[n] - Q_{K_i^n}^{user} \|^2} \right), \tag{33}$$

here, $\mathbf{Q}^{uav}[n]$ denotes the UAV's position coordinates at the first time slot, $\mathbf{Q}_{K_i^n}^{user}$ is the position coordinates of user K_i^n, and $\|\bullet\|$ means the Euclidean distance. Therefore, equation (31) can be calculated as

$$\begin{aligned} \tilde{T}_{t,K_i^n}^{user}[n] &= \frac{\lambda_{K_i^n}[n] D_{K_i^n}[n]}{r_{K_i^n}[n]} \\ s.t. \quad & C10^*: r_{K_i^n}[n] \le \hat{R}_{K_i^n}[n], C11. \end{aligned} \tag{34}$$

Next, we utilize SCA method and introduce Lemma 1 to facilitate the transformation.

Lemma 1: By applying SCA, substituting $\hat{R}^*_{K_i^n}[n]$ and $\| \tilde{h}_{K_i^n}[n] \|^2$ with $\hat{R}_{K_i^n}[n]$ and $\| h_{K_i^n}[n] \|^2$, equation (34) is transformed into a standard convex programming problem. Define $Z_{K_i^n}[n] = \| \mathbf{Q}^{uav}[n] - \mathbf{Q}_{K_i^n}^{user} \|^2$, and let $\hat{R}^*_{K_i^n}[n]$ be the first-order Taylor expansion of $\hat{R}_{K_i^n}[n]$ at $\tilde{Z}_{K_i^n}[n]$:

$$\hat{R}^*_{K_i^n}[n] = A_{K_i^n}[n] - (Z_{K_i^n}[n] - \tilde{Z}_{K_i^n}[n]) B_{K_i^n}[n], \tag{35}$$

where $A_{K_i^n}[n] = B \log_2 \left(1 + \frac{P_{K_i^n}[n] \alpha_0^{LoS}}{(\chi_t[n] + \sigma^2) \tilde{Z}_{K_i^n}[n]} \right) \ge 0$, $B_{K_i^n}[n] = \frac{P_{K_i^n}[n] \alpha_0^{LoS} B \log_2 e}{(\tilde{Z}_{K_i^n}[n])^2 (\chi_t[n] + \sigma^2) + \tilde{Z}_{K_i^n}[n] P_{K_i^n}[n] \alpha_0^{LoS}} \ge 0$.

Similarly, $\|\tilde{h}_{K_i^n}[n]\|^2$ is the first-order Taylor expansion of $\| h_{K_i^n}[n] \|^2$ at $\tilde{Z}_{K_i^n}[n]$:

$$\begin{aligned} \|\tilde{h}_{K_i^n}[n]\|^2 =& D_{K_i^n}[n] - E_{K_i^n}[n](x^{uav}[n] - \tilde{x}^{uav}[n]) \\ & - F_{K_i^n}[n](y^{uav}[n] - \tilde{y}^{uav}[n]), \end{aligned} \tag{36}$$

where $D_{K_i^n}[n] = \frac{\alpha_0^{LoS}}{\tilde{Z}_{K_i^n}[n]}$, $E_{K_i^n}[n] = \frac{2\alpha_0^{LoS}(\tilde{x}^{uav}[n] - x_{K_i^n}^{user})}{\left(\tilde{Z}_{K_i^n}[n]\right)^2}$, $F_{K_i^n}[n] = \frac{2\alpha_0^{LoS}(\tilde{y}^{uav}[n] - y_{K_i^n}^{user})}{\left(\tilde{Z}_{K_i^n}[n]\right)^2}$.

Here, $\tilde{Z}_{K_i^n}[n]$ stands for the optimal value from the last iteration, i.e., $\tilde{Z}_{K_i^n}[n] = \| \tilde{\mathbf{Q}}^{uav}[n] - \mathbf{Q}_{K_i^n}^{user} \|^2$, where $\tilde{\mathbf{Q}}^{uav}[n] = (\tilde{x}^{uav}[n], \tilde{y}^{uav}[n], h^{uav})$.

Proof: For a differentiable function $f(x)$, it can be approximated by its tangent function at point x_0 as $g(x, x_0)$, which is the first-order Taylor expansion of $f(x)$ at x_0. Thus, we have:

$$f(x) \geq g(x, x_0) = f(x_0) + (x - x_0)f'(x_0), \tag{37}$$

where $f'(x_0)$ is the first order derivative of $f(x)$ at x_0. The equality holds when $x = x_0$. After a first-order Taylor expansion, the function $f(x)$ becomes $g(x, x_0) = f(x_0) + (x - x_0)f'(x_0)$, making $g(x, x_0)$ an affine function. ■

In equation (35), $\hat{R}^*_{K_i^n}[n]$ is an affine function with respect to $Z_{K_i^n}[n]$, and $Z_{K_i^n}[n]$ is convex concerning $\mathbf{Q}^{uav}[n]$. Thus, $\hat{R}^*_{K_i^n}[n]$ is a concave function concerning $\mathbf{Q}^{uav}[n]$, which makes constraint $C10^*$ a standard convex constraint. Meanwhile, in equation (36), $\|\tilde{h}_{K_i^n}[n]\|^2$ is affine concerning $\mathbf{Q}^{uav}[n]$, thus making constraint $C11^*$ a standard convex constraint as well. Therefore, equation (34) is transformed into a standard convex programming problem, defined as

$$\begin{aligned} &\tilde{T}^{user}_{t,K_i^n}[n] = \frac{\lambda_{K_i^n}[n] D_{K_i^n}[n]}{r_{K_i^n}[n]} \\ s.t. \quad &C10^*: r_{K_i^n}[n] \leq \hat{R}^*_{K_i^n}[n], \\ &C11^*: \sum_{i=1}^{S-1} P_{K_i^n}[n] \|\tilde{h}_{K_i^n}[n]\|^2 \leq \chi_t[n]. \end{aligned} \tag{38}$$

In equation (29), in addition to the objective function and constraint $C8$ being non-convex, $C7$ in the constraint is also non-convex. Constraint $C7$ represents the energy consumption constraint of the UAV, whereby the sum of the UAV's flight and computational energy consumption during the cycle must be less than or equal to its energy gained through the LWPT. As the LWPT channel between the UAV and the PB is subject to change, this also causes the LWPT function to be non-convex. The constraint $C7$ in subproblem **SP4** presents a significant challenge due to the high coupling of variables, rendering it non-convex. To address this, we use the same SCA method. Consequently, we have:

$$C7^*: E^{fly}[n] + E^{uav}_{c,K_i^n}[n] \leq E^{uav}_0 + \tilde{E}_{eh}[n], n \in N. \tag{39}$$

This transformation converts $C7^*$ into a convex constraint.

In equation (29), $E^{user}_{t,K_i^n}[n]$ in constraint $C8$ of subproblem **SP4** has a similar form to the objective function and can be transformed in a manner analogous to equation (38):

$$\begin{aligned} &\tilde{E}^{user}_{t,K_i^n}[n] = \frac{P_{K_i^n}[n] \lambda_{K_i^n}[n] D_{K_i^n}[n]}{r_{K_i^n}[n]} \\ s.t. \quad &C10^*, C11^*. \end{aligned} \tag{40}$$

This reformulation ensures that constraint $C8$ becomes convex.

As a result, the previously non-convex objective function and constraints in **SP4** are transformed into a convex objective function and constraints, thereby reformulating the original problem **SP4** into:

$$\begin{aligned} &\mathbf{SP4}^*: \min_{\boldsymbol{Q}^{uav}} \sum_{n=1}^{N} \tilde{t}_{K_i^n}[n] \\ s.t. \quad &C1^*, C5, C6, C7^*, C8^*, C9^*, C10^*, C11^*. \end{aligned} \tag{41}$$

SP4* is now a convex optimization problem that can be solved using standard convex optimization tools such as CVX [76]. The detailed solution procedure is outlined in Algorithm 3.

Algorithm 3 MEC network UAV trajectory optimization

1: Initialize UAV trajectory $\tilde{\boldsymbol{Q}}^{uav}$, the number of iterations $l = 0$, and initial utility ζ_0. Get $\boldsymbol{\lambda}$, $\mathbf{P}_b$ by solving $\mathbf{SP3}^*$.
2: **Repeat**
3: Update $\mathbf{K}^*$ via Algorithm 1.
4: For $\boldsymbol{\lambda}$, $\mathbf{P}_{as}$ and $\mathbf{K}^*$, solve subproblem $\mathbf{SP4}^*$ to obtain $\zeta_{l+1} = \underset{\boldsymbol{Q}^{uav}}{argmin} \sum_{n=1}^{N} \tilde{t}_{K_i^n}[n]$.
5: $\tilde{\boldsymbol{Q}}^{uav} = \boldsymbol{Q}^{uav}$, $l = l + 1$
6: **Until** Convergence or the maximum number of iterations is satisfied.
7: Output: $\boldsymbol{Q}^{uav}$.

The above describes the solution process for the two subproblems. For subproblem $\mathbf{SP3}$, since it is a convex optimization problem, the solution obtained is the optimal solution. For subproblem $\mathbf{SP4}$, due to the constant changes in the UAV's trajectory, the channels between the UAV, ground users, and the PB are also continuously varying, making $\mathbf{SP4}$ a non-convex optimization problem. In this paper, we propose an optimization algorithm based on the SCA framework to solve $\mathbf{SP4}$. Due to the convergence properties of the SCA algorithm, at least a suboptimal solution can be obtained for $\mathbf{SP4}$. The joint optimization algorithm is presented below.

C. Joint Optimization Algorithm for Resource Allocation and UAV Trajectory

In the paper, problem $\mathbf{P1}$ is decomposed into two convex subproblems, (28) and (41). By iteratively solving these subproblems, we achieve resource allocation and joint optimization of UAV trajectories. Algorithm 1 updates $\mathbf{K}^*$ after each iteration, enabling us to iteratively solve the original problem $\mathbf{P1}$ using Algorithm 4. The performance of Algorithm 4 depends on the initial UAV trajectory $\tilde{\boldsymbol{Q}}^{uav}$. In our proposed approach, we use a circular trajectory centered at the user's position, ensuring uniform coverage of all users and maximizing fairness.

Algorithm 4 Joint alternating optimization algorithm for resource allocation and UAV trajectories

1: Initialize UAV trajectory $\tilde{\boldsymbol{Q}}^{uav}$, the number of iterations $l = 0$, and optimal solution ρ_0.
2: **Repeat**
3: Update $\mathbf{K}^*$ via Algorithm 1.
4: For $\tilde{\boldsymbol{Q}}^{uav}$, solve (28) to get the $\boldsymbol{\lambda}$, $\mathbf{P}_b$.
5: Using $\boldsymbol{\lambda}$, $\mathbf{P}_b$, solve (41) to get the $\mathbf{Q}^{uav}$.
6: For $\boldsymbol{\lambda}$, $\mathbf{P}_b$, $\boldsymbol{Q}^{uav}$, get the optimal solution ρ_{l+1}.
7: $\tilde{\boldsymbol{Q}}^{uav} = \boldsymbol{Q}^{uav}$, $l = l + 1$.
8: **Until** Convergence is satisfied.

In the actual deployment process, the alternating optimization framework described in Algorithm 4 relies on Algorithm

1 to obtain users' CSI and generate user scheduling decisions accordingly. In each iteration of the alternating optimization, when the UAV flies according to the optimized trajectory in each time slot, ground users within the coverage range of its current position will actively report their location information and key task parameters. Given that most users in our studied scenario are sensor nodes with fixed positions or slow mobility, users' CSI can be largely inferred or estimated from their reported positions.

Furthermore, since the UAV serves S users in each time slot, it is not necessary to obtain complete CSI of all users. Only the instantaneous CSI of several key users that are relatively close to the UAV and have significant impact on system performance needs to be collected. Based on the CSI information of these users, effective user scheduling decisions can be obtained through Algorithm 1.

The CSI acquisition strategy we implement ensures both the rationality and real-time performance of scheduling decisions while avoiding dependence on global CSI, thereby significantly reducing system communication overhead and enhancing the deployability of the algorithm in practical scenarios.

The convergence and computational complexity of Algorithm 4 are discussed in Remarks 1 and 2, respectively.

Convergence Analysis: For Algorithm 4 to converge, it is essential that each subproblem derived from the original problem is solved optimally in every iteration. In this study, subproblem 1, addressed in step 4 of Algorithm 4, is a linear programming problem. For the initial UAV trajectory $\{\tilde{\boldsymbol{Q}}^{uav}\}$, the optimal values for $\{\boldsymbol{\lambda}, \mathbf{P}_b\}$ can be determined by solving subproblem (28). In subproblem 2, T_{total} is defined as the optimal value of the objective function for the original problem with respect to $\{\boldsymbol{\lambda}, \mathbf{P}_b, \boldsymbol{Q}^{uav}\}$, while T_2 represents the objective function in subproblem 2 $\{\boldsymbol{\lambda}, \mathbf{P}_b\}$ and $\{\boldsymbol{Q}^{uav}\}$. Since subproblem (28) is a linear programming problem, and the UAV trajectory $\boldsymbol{Q}^{uav}$ is optimal, we have:

$$T_{total}(\boldsymbol{\lambda}^l, (\boldsymbol{Q}^{uav})^l, \mathbf{P}_b^l) \leq T_{total}(\boldsymbol{\lambda}^{l+1}, (\boldsymbol{Q}^{uav})^l, \mathbf{P}_b^{l+1}). \quad (42)$$

In step 5 of Algorithm 4, it follows that:

$$\begin{aligned} T_{total}(\boldsymbol{\lambda}^l, (\boldsymbol{Q}^{uav})^l, \mathbf{P}_b^l) &= T_2(\boldsymbol{\lambda}^{l+1}, (\boldsymbol{Q}^{uav})^l, \mathbf{P}_b^{l+1}) \\ &\leq T_2(\boldsymbol{\lambda}^{l+1}, (\boldsymbol{Q}^{uav})^{l+1}, \mathbf{P}_b^{l+1}), \end{aligned} \quad (43)$$

because the first-order Taylor expansion at any local point is exact, and since Equation (41) is a strictly convex optimization problem with a unique solution in each iteration, the inequality holds. Furthermore, the objective value in (41) at step 4 serves as a lower bound for the objective value of the original problem, implying:

$$T_2(\boldsymbol{\lambda}^{l+1}, (\boldsymbol{Q}^{uav})^{l+1}, \mathbf{P}_b^{l+1}) \leq T_{total}(\boldsymbol{\lambda}^{l+1}, (\boldsymbol{Q}^{uav})^{l+1}, \mathbf{P}_b^{l+1}). \quad (44)$$

Thus, Algorithm 4 is guaranteed to converge to at least a locally optimal solution. Fig. 2 demonstrates the trend of system delay reduction across different values of S as the number of iterations increases. The delay consistently decreases with more iterations, achieving convergence after roughly eight iterations.

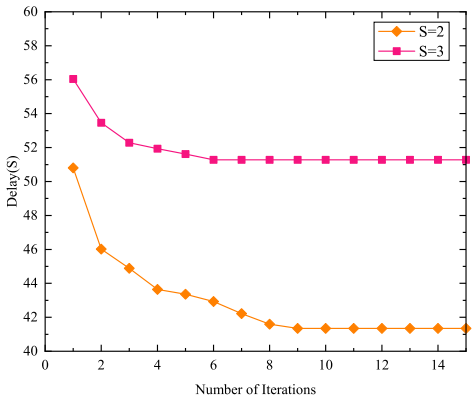

Fig. 2. Algorithm 4 convergence for different S.

Computational Complexity Analysis: The complexity of Algorithm 4 encompasses several components: updating $\mathbf{K}^*$ in Algorithm 1 and solving the optimization problems (28) and (41). The inner loop in Algorithm 1 executes $M \times N$ times, resulting in a complexity of $\mathcal{O}(MN)$. Both problems (28) and (41) are linear programming problems solved in each iteration of Algorithm 4 with a complexity of $\mathcal{O}(n_L^2 m_L)$ [75], where n_L is the number of optimization variables and m_L is the number of constraints. For problem (28), $n_L = (2M+1)N$ and $m_L = (4S+M+1)N$, yielding a complexity of $\mathcal{O}(L_{P_1}((4S+M+1)(2M+1)^2N^3))$, where L_{P1} represents the number of iterations needed to solve (30). Similarly, the complexity of solving problem (41) is $\mathcal{O}(L_{P2}((2M+S+2)(2M+2)^2N^3))$, with L_{P2} denoting the iterations required to solve (41). Thus, the overall computational complexity of Algorithm 4 can be expressed as: $O(L_{TO}(MN + L_{P1}((4S+M+1)(2M+1)^2N^3) + L_{P2}((2M+S+2)(2M+2)^2N^3)))$, where L_{TO} is the number of iterations required for Algorithm 4 to converge.

*Implementability Analysis:*The proposed algorithm features nested (inner–outer) iterations. In the UAV trajectory optimization stage, SCA iterations are executed in the inner loop to handle nonconvexity; however, the number of SCA iterations cannot be determined a priori, which increases the overall computational burden and hinders practical deployment. To alleviate this, lower-complexity SCA approximations can be used. Although such approximations may reduce solution accuracy, they substantially cut computational cost and thus improve deployability. Specifically, Stochastic SCA (SSCA) [77] requires solving only a single, consistently feasible convex surrogate per iteration. This reduces the number of convex solves per iteration from as many as two to just one and, despite a modest loss in accuracy, significantly accelerates convergence and lowers total computational complexity. Accelerated SCA (ASCA) [78] reformulates the SCA update as a fixed-point nonlinear equation and employs Newton-type methods (or their variants) to rapidly find the root of that equation, thereby speeding up convergence.

V. Numerical Results and Analysis

In this section, we present the results of our simulation experiments, which are designed to evaluate the effectiveness

of the proposed scheme relative to both the baseline OMA scheme and several established heuristics. First, we examine the optimization performance of our system under the configurations detailed below. Next, we conduct a comprehensive comparison against the OMA scheme and the algorithms introduced in [79]–[83], namely, the Dandelion Optimizer Algorithm (DOA) [79], the Komodo Mlipir Algorithm (KMA) [80], Adaptive Exploration-based State-Space Particle Swarm Optimization (AESSPSO) [81], Linear Subspace Surrogate Modeling for Large-Scale Expensive Single-Objective Optimization (L2SMEA) [82], and Surrogate-Assisted Differential Evolution with Adaptive Multisubspace Search for Large-Scale Expensive Optimization (SADEAMSS) [83]. Finally, we analyze how key system parameters influence overall performance, highlighting the robustness and adaptability of our approach.

The system comprises a UAV equipped with an edge server, a PB, and $M = 8$ users uniformly distributed over an area of $1000 \times 1000m^2$. In scenarios such as disaster monitoring, environmental sensing, or infrastructure inspection, ground users are typically sensors, base stations, or rescue stations installed at fixed locations. Their physical positions remain almost constant during the task execution cycle. Therefore, considering them as stationary nodes accurately reflects the actual system. Consequently, we assume that the users' locations change slowly or not at all within a system time slot.

We assume that the UAV's flight altitude is the same as that of the PB, denoted as $h^{uav} = h^{as} = 30m$. The mission duration is $T = 100$ s, divided into $N = 20$ equal time slots. Each of the $S = 2$ ground users transmits with power $P = 0.2$ W over a bandwidth $B = 10^7$ Hz, the uplink noise power is $\sigma^2 = -120$ dBm and the reference channel gain at 1 m is $\alpha_0^{LoS} = -40$ dB. Every user has a data load of $D_{K_i^n} = 5 \times 10^6$ bits per slot, and both the UAV and users require $C = 10^3$ CPU cycles per bit. The local CPU frequency at each user is $f_{K_i^n}^{user} = 10^9$ Hz, while the UAV's edge server runs at $f^{uav} = 3 \times 10^9$ Hz, the effective switching capacitance is $\kappa^{uav} = \kappa_{K_i^n}^{user} = 10^{-29}$. The UAV's energy consumption rate during flight is characterized by $\eta = 10^{-4}$, with vehicle mass $W^{uav} = 10$ Kg and maximum speed $V_{\max}^{uav} = 12$ m/s. Laser power transfer is modeled with a PB transmit peak power of 60 W, telescope aperture $A = 5 \times 10^{-3}\mathrm{m}^2$, beam diameter $D = 0.1$ m, angular spread $\Delta\theta = 3.4 \times 10^8$ rad, optical efficiency $\chi = 1.5\mathrm{Lm/W}$, channel attenuation $\alpha_1 = 10^{-6}\mathrm{m}^{-1}$, and energy-conversion efficiency $\beta = 0.9$.

As shown in Fig. 3, the link channel conditions between the UAV and ground users fluctuate across different time slots due to the changing position of the UAV. The UAV leverages its maneuverability to adaptively adjust its trajectory based on user scheduling strategy in Algorithm 1, thereby improving channel conditions with ground users and enhancing the quality of service.

Fig. 4 depicts the task offloading ratio for each time slot. We assume that two users can offload the task to the UAV via the uplink NOMA at any given time. In each time slot, the two users with the best channel conditions offload tasks to the UAV. For example, in slots 17 to 19, users 7 and 8, being closest to the UAV, offload tasks while others execute them locally. In the final slot, as the UAV approaches users 4 and 7, they gain network access, while user 8 no longer offloads tasks.

Fig. 5 illustrates the optimization results of the PB transmission power in each time slot. Combining this with Fig. 3, we can deduce that when the UAV is in close proximity to the PB, the wireless energy transfer conditions between the

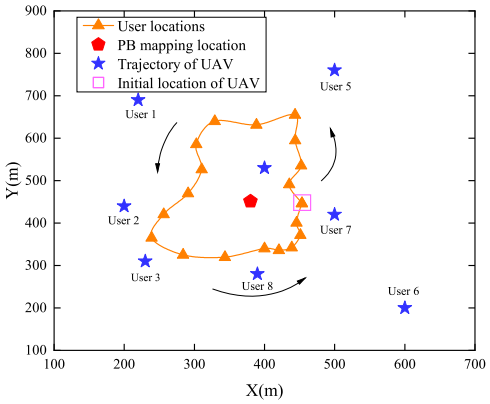

Fig. 3. UAV trajectory (The direction of the black arrow is the direction of the trajectory).

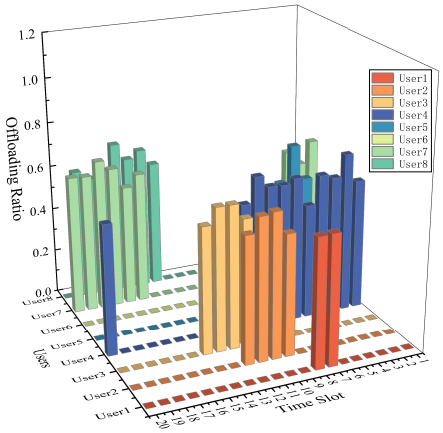

Fig. 4. User offloading ratio per time slot.

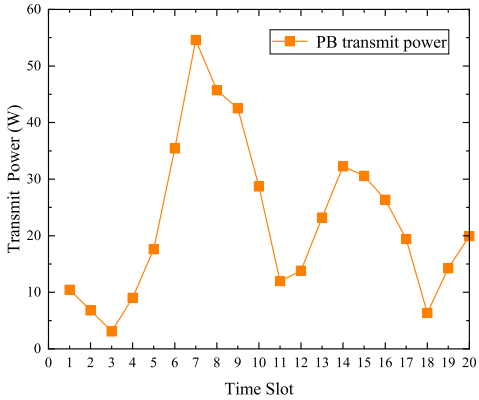

Fig. 5. Transmit power of PB.

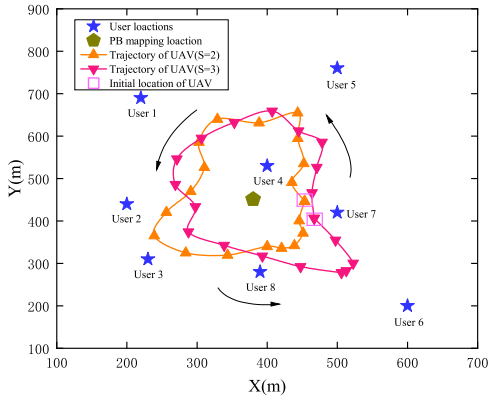

Fig. 6. Comparison of UAV trajectories for $S = 2$ and $S = 3$. (The direction of the black arrow is the direction of the trajectory)

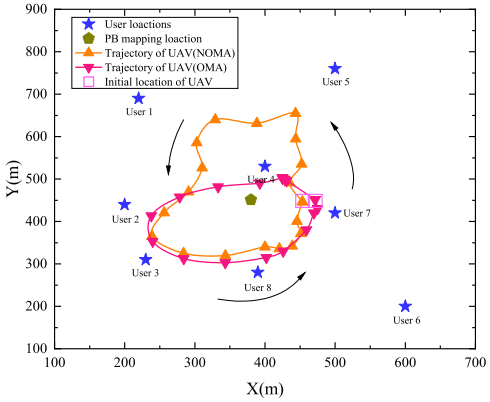

Fig. 7. Comparison of UAV trajectories between the NOMA and OMA schemes. (The direction of the black arrow is the direction of the trajectory)

PB and the UAV can be enhanced, resulting in a decrease in the transmission power of the PB. Because the UAV depends on the LWPT technique to recharge its batteries from the PB in order to sustain cruise flight and perform computing tasks, its energy limitations impose restrictions on its range from the PB. As the UAV moves farther, the PB needs to increase its transmission power to meet the UAV's energy needs.

To further evaluate the trajectory optimization performance of the proposed algorithm, we set the number of serviceable users connected to the UAV's uplink NOMA network to three(denoted as $S = 3$). While the UAV's trajectory coverage is extensive, it still needs to adjust its path to serve a larger number of ground users. Fig. 6 demonstrates the comparison of UAV trajectory optimization results for different numbers of access users. From this figure, it is clear that the proposed algorithm can flexibly optimize the UAV's trajectory by considering the varying number of served users.

To demonstrate the advantages of our proposed approach, we introduce a reference system for comparison. This reference system is identical to the proposed system except that it employs OMA instead of NOMA for task offloading. Assuming no interference, the bandwidth allocated to each user in the OMA system is reduced to $1/S$ of that in the NOMA scenario. The transmission rate of each user in the n^{th} time slot is given by [18]:

$$R_{K_i^n}^{OMA}[n] = (B/S)\log_2\left(1 + \frac{P_{K_i^n}[n] \parallel h_{K_i^n}[n] \parallel^2}{\sigma^2/S}\right). \quad (45)$$

The methodology for solving the OMA scheme parallels our approach for NOMA, with necessary adjustments for device scheduling.

Fig. 7 illustrates a comparison between the optimized trajectories for NOMA and OMA scenarios for UAV. The two scenarios exhibit a clear contrast, as the NOMA scenario offers a wider coverage compared to the OMA scenario, which has a narrower range and is unable to efficiently serve multiple ground users. The reduced range of the UAV trajectory in the OMA scenario is caused by the fact that the OMA scheme only considers users with strong channel conditions who are in close proximity to the UAV while ignoring those who are

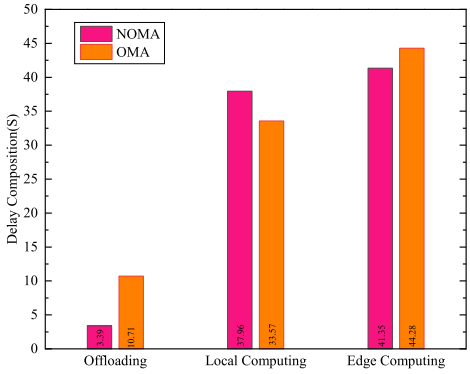

Fig. 8. Comparison of optimization results between NOMA and OMA schemes.

farther away. Furthermore, in the OMA scenario, users located farther away experience increased "costs" when delegating tasks to the UAV. Conversely, the NOMA scheme provides wider coverage, allowing it to serve a greater number of users.

Fig. 8 depicts the delay performance of offloading jobs for the proposed algorithm in both NOMA and OMA. For NOMA, the offloading delay is 3.39 seconds, and the total system delay is 41.35 seconds (3.39 + 37.96). For OMA, the offloading delay is 10.71 seconds, and the total system delay is 44.28 seconds, which is the sum of the offloading delay (10.71 seconds) and the remaining delay (33.57 seconds). The results demonstrate that the proposed algorithm in the NOMA scenario achieves a significant 68.3% decrease in offloading delay and a noteworthy enhancement in the overall system delay when compared to the OMA scenario. One reason for this is that NOMA technology allows users to utilize the same spectrum resources, resulting in improved channel conditions and reduced delays when ground users offload tasks to the UAV.

Fig. 9 illustrates the distribution of system delay for varying numbers of users served. As the user number increases, both systems experience higher delays. However, the NOMA system consistently outperforms the OMA system in terms of system delay. This discrepancy expands as the number of users

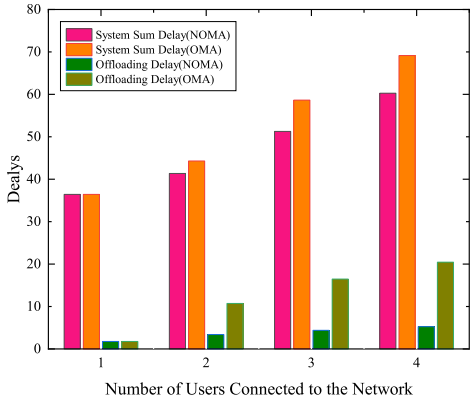

Fig. 9. Comparison of results with different numbers of access users.

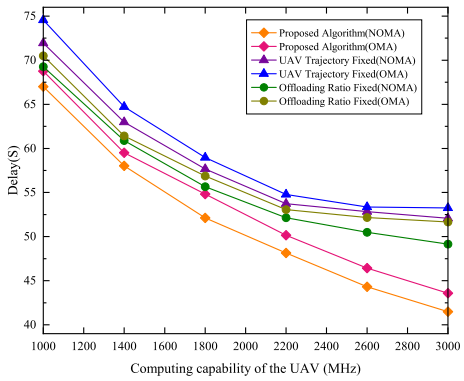

Fig. 11. Optimization results of different schemes with different UAV computing power.

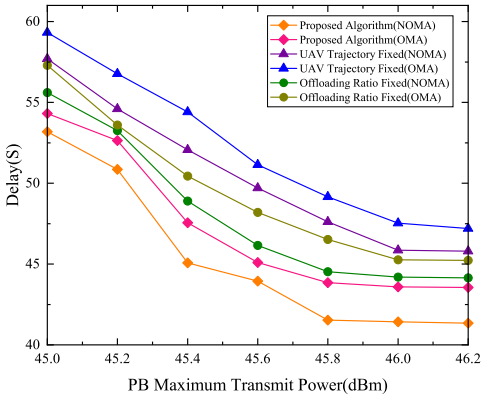

Fig. 10. Optimization results of different schemes with different PB transmit power thresholds.

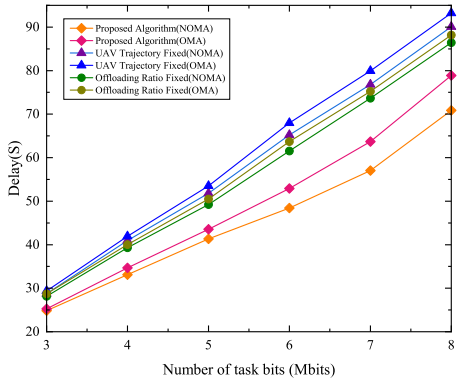

Fig. 12. Optimization results for different scenarios with different task volumes.

increases. Furthermore, as illustrated in Fig. 9, the offloading delay-to-user ratio in the NOMA system is considerably lower than that in the OMA system. This indicates that the NOMA improves the overall system delay by reducing offloading delay, leading to a corresponding reduction in total system delay.

To comprehensively evaluate the proposed UAV-assisted NOMA algorithm, we analyze its impact on system delay under varying PB transmit-power thresholds, task sizes, UAV computing capabilities, and transmission bandwidths. Under both NOMA and OMA access schemes, we compare the proposed algorithm with a predetermined UAV flight trajectory having a fixed offloading ratio, and in the same scenario benchmark it against five heuristic algorithms to demonstrate its superiority in the constructed network system.

We first studied how different PB transmit power thresholds affect system delay. Fig. 10 shows the delay for NOMA, OMA, and four baseline schemes as the threshold increases for a fixed task size. As the PB power threshold rises, all schemes see reduced delay because the UAV's MEC server can process tasks more quickly with more energy. Our proposed algorithms achieve the lowest delays by dynamically optimizing UAV trajectories and task-offloading ratios. Beyond a certain power level, delay improvements plateau, showing the UAV has reached its energy capacity. These results confirm that our methods not only minimize delay but also enhance energy efficiency.

Fig. 11 and Fig. 12 demonstrate the delay performance for various UAV computing power levels and computational task sizes, respectively. These results show that the proposed algorithm outperforms other algorithms, and its advantages become more pronounced as the parameters change. The optimization curves in Fig. 11 show that as UAV computing power increases, it encourages users to offload more tasks to the MEC server and reduces overall system delay. Our proposed algorithm better balances offloading and computation delays, thereby improving the overall system performance. In contrast, other algorithms do not effectively balance system delay. Fig. 12 shows a similar trend. Fig. 12 illustrates that as the size of computational tasks increases, so does the overall system delay. However, because the coupling of variables in our proposed algorithm changes the overall system delay composition, its delay remains significantly lower than that of other algorithms.

The result curves in Fig. 11 and Fig. 12 corroborate each other and confirm the obvious advantage of our proposed algorithm. Furthermore, these results demonstrate that the proposed algorithms can effectively optimize the UAV trajectory, PB transmit power, and task offloading to achieve the desired delays. As a result, the above-mentioned results show that our

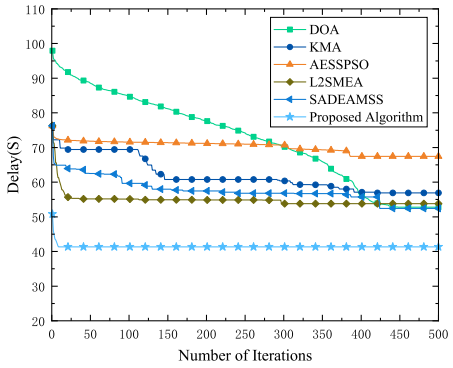

Fig. 13. Comparison of convergence of different algorithms.

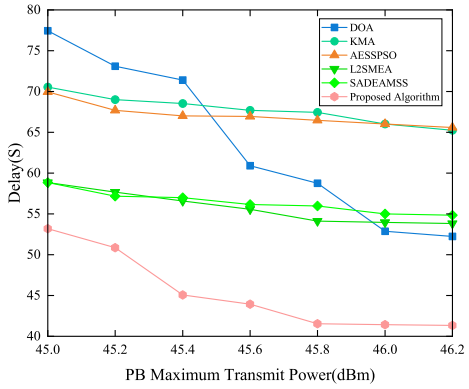

Fig. 14. Optimization results of different algorithms at different PB transmit power thresholds.

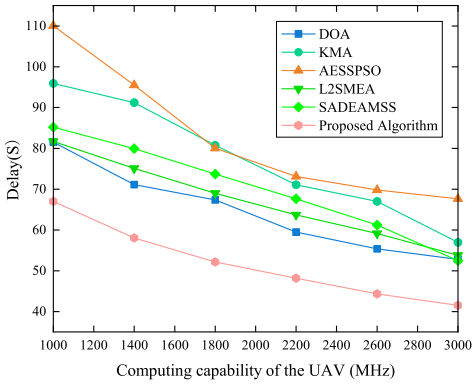

Fig. 15. Optimization results of different algorithms at different UAV computing power.

proposed UAV-assisted NOMA scheme outperforms conventional OMA approaches across a wide range of operational scenarios and parameters.

In Fig. 13, all five heuristic algorithms show the same trend: delay falls quickly with iterations and then levels off. DOA and KMA converge slowest with the highest final delay; AESSPSO is slightly better; L2SMEA and SADEAMSS outperform others in later iterations thanks to stronger local fine-tuning. By contrast, the proposed alternating-optimization algorithm attains the lowest delay at every iteration, converges fastest, and achieves significantly better steady-state performance. These benefits arise from its decomposition into precisely solved convex subproblems and its rigorous convergence properties.

Although heuristics have lower per-iteration cost, they need many iterations and are prone to local optima and large fluctuations. The alternating-optimization method, despite higher per-iteration complexity, converges rapidly and stably within few iterations, yielding markedly superior convergence speed and system delay.

Fig. 14 illustrates the performance curves of different algorithms as the PB transmission power gradually increases. As the maximum PB transmission power rises, the system delay of all algorithms decreases rapidly and then gradually stabilizes. Among these algorithms, DOA and KMA, which prioritize global search but lack local fine-tuning capabilities, demonstrate the highest delay at lower transmission powers. AESSPSO achieves reasonable performance at lower transmission powers through particle swarm optimization and local search; however, its performance gradually degrades as transmission power increases. L2SMEA and SADEAMSS, relying on diverse mutation and crossover operations, exhibit stronger fine-tuning capabilities at higher transmission power levels and maintain relatively stable performance. The proposed algorithm, by jointly optimizing two sub-convex problems, not only quickly identifies the optimal region but also precisely converges to a lower delay, consistently outperforming all heuristic algorithms.

In Fig. 15, the delay optimization curves of each algorithm under different UAV computing capabilities all decrease significantly as computing power increases—this is because stronger computing power can accelerate task processing on the UAV side, reduce computational delay, and thereby drive down the overall system delay. Among the five heuristic algorithms, DOA performs best in low-computing-power environments, indicating that it can still efficiently allocate tasks even under resource-constrained conditions; but its performance remains inferior to the algorithm proposed in this paper regardless of computational power. AESSPSO and KMA exhibit similar performance, with KMA slightly outperforming AESSPSO in high computational power ranges, primarily due to AESSPSO's tendency to converge prematurely under high computational power; meanwhile, KMA exhibits significant fluctuations in low computational power ranges, indicating its sensitivity to parameter settings. SADEAMSSO and L2SMEA exhibit similar performance at medium to high computing power levels, but both experience significant delay spikes at low computing power levels. In contrast, the algorithm proposed in this paper consistently outperforms the above five methods and can more fully utilize additional resources as computing power increases, effectively reducing computational and communication overhead to achieve more significant delay optimization.

Fig. 16 shows the optimization curves of different algorithms under varying task scales. As the user task scale increases, system delay exhibits a nearly linear upward trend, with the slopes of different algorithms reflecting their differing capabilities in handling high loads. DOA and KMA experience

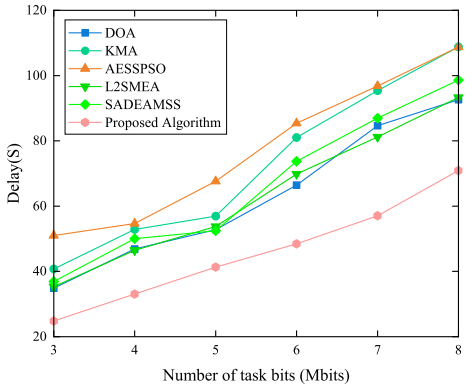

Fig. 16. Optimization results of different algorithms at different task volumes.

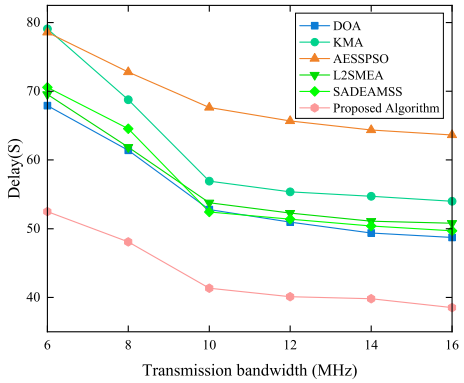

Fig. 17. Optimization results of different algorithms at different Transmission bandwidth.

a significant surge in delay even with a slight increase in task volume, indicating that global exploration is insufficient to handle high loads. AESSPSO, L2SMEA, and SADEAMSS achieve gradual optimization in slope through hybrid strategies and adaptive evolution, respectively, with L2SMEA showing relatively stable performance, the algorithm proposed in this paper demonstrates the smallest slope growth due to its refined joint scheduling and resource allocation design, maintaining a relatively flat delay increase even when task scale increases dramatically.

Fig. 17 illustrates the optimization curves of various algorithms under different transmission bandwidth conditions. As bandwidth increases, the performance of all algorithms improves significantly. This is primarily attributed to higher bandwidth enabling the transmission of more data and reducing the probability of channel congestion, thereby enhancing the system's transmission efficiency. The DOA algorithm demonstrates stable and superior optimization performance across all bandwidth levels, primarily due to its deterministic search strategy, which enables it to quickly locate local or global optimal solutions. In contrast, the KMA and AESSPSO algorithms, leveraging clustering mechanisms and particle swarm characteristics, can also rapidly reduce system delay as bandwidth increases. However, due to their tendency to get stuck in local optima, their overall performance still lags behind that of the DOA algorithm. The L2SMEA and SADEAMSS algorithms perform at an intermediate level. While their adaptive mechanisms can balance exploration and exploitation to some extent, they have not completely overcome the issue of premature convergence, resulting in poorer performance than the proposed algorithm in high-bandwidth scenarios. Notably, the proposed algorithm maintains optimal performance under all bandwidth conditions, even at low bandwidth, its performance approaches that of other comparison algorithms at high bandwidth, fully demonstrating the robustness and superiority of the proposed scheme.

Fig. 18 shows the delay optimization curves of each algorithm under different user offload power conditions. As the user offload power increases, the changes in delay for each algorithm are relatively gradual, with only minor fluctuations within a certain range and no sudden jumps. This is primarily due to the small energy storage units equipped on ground

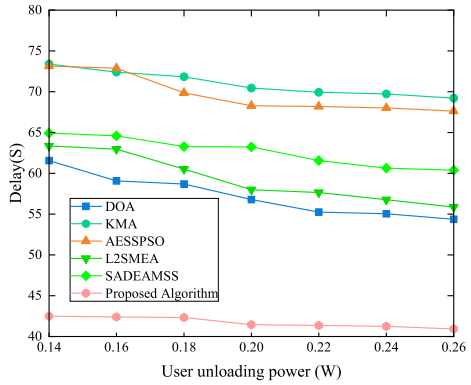

Fig. 18. Optimization results of different algorithms at different User transmit power.

users, which can cache and smooth the instantaneous energy transmitted by the UAV via RF-WPT. As a result, even if the UAV's transmission power or channel conditions fluctuate slightly within a time slot, the user's actual transmission power remains stable. Additionally, since the scheduling time slot duration is brief, the relative positions between the UAV and ground users remain nearly constant within a single time slot. According to the free-space propagation model, the intra-slot fluctuations in channel gain can be neglected, so the minor fluctuations in transmission power have minimal impact on the system's overall delay.

VI. CONCLUSION AND FUTURE WORK

This paper proposes a LWPT-based uplink NOMA UAV-assisted MEC system for task offloading, aiming to minimize system delay over the entire operation cycle by jointly optimizing the task offloading ratio, PB transmit power, and UAV trajectory. Due to the non-convex nature of the problem, an alternating optimization algorithm based on the SCA framework is developed. A user scheduling strategy is first introduced to enhance UAV trajectory planning and channel conditions, thereby reducing problem complexity. The original problem is then decomposed into two subproblems, which are iteratively solved to obtain the optimal solution.

Simulation results demonstrate that the proposed algorithm significantly outperforms the OMA scheme in reducing delay and improving user capacity. Specifically, it achieves a 68.3% reduction in offloading delay, with performance gains increasing under heavier computational loads. The results verify that the proposed method not only yields a feasible UAV trajectory but also enhances delay performance and energy efficiency. Future work will expand to multi-UAV collaborative systems based on the existing framework by introducing dynamic user-UAV association mechanisms, hierarchical optimization strategies, power constraint management, and multi-UAV scheduling models to meet the needs of larger-scale and more complex service scenarios.

REFERENCES

[1] Y. Qu et al., "Service Provisioning for UAV-Enabled Mobile Edge Computing," *IEEE J. Sel. Areas Commun.*, vol. 39, no. 11, pp. 3287-3305, Nov. 2021.

[2] P. McEnroe, S. Wang and M. Liyanage, "A Survey on the Convergence of Edge Computing and AI for UAV: Opportunities and Challenges," *IEEE Internet Things J.*, vol. 9, no. 17, pp. 15435-15459, Sep. 2022.

[3] P. Zhang, C. Wang, C. Jiang and A. Benslimane, "UAV-Assisted Multi-Access Edge Computing: Technologies and Challenges," *IEEE Internet Things Mag.*, vol. 4, no. 4, pp. 12-17, Dec. 2021.

[4] D. Callegaro and M. Levorato, "Optimal Edge Computing for Infrastructure-Assisted UAV Systems," *IEEE Trans. Veh. Technol.*, vol. 70, no. 2, pp. 1782-1792, Feb. 2021.

[5] T. Zhang, Y. Xu, J. Loo, D. Yang and L. Xiao, "Joint Computation and Communication Design for UAV-Assisted Mobile Edge Computing in IoT," *IEEE T IND INFORM.*, vol. 16, no. 8, pp. 5505-5516, Aug. 2020.

[6] Z. Yu, Y. Gong, S. Gong and Y. Guo, "Joint Task Offloading and Resource Allocation in UAV-Enabled Mobile Edge Computing," *IEEE Internet Things J.*, vol. 7, no. 4, pp. 3147-3159, Apr. 2020.

[7] T. Bai, J. Wang, Y. Ren and L. Hanzo, "Energy-Efficient Computation Offloading for Secure UAV-Edge-Computing Systems," *IEEE Trans. Veh. Technol.*, vol. 68, no. 6, pp. 6074-6087, Jun. 2019.

[8] A. Kiani and N. Ansari, "Edge Computing Aware NOMA for 5G Networks," *IEEE Internet Things J.*, vol. 5, no. 2, pp. 1299-1306, Apr. 2018.

[9] L. P. Qian, A. Feng, Y. Huang, Y. Wu, B. Ji and Z. Shi, "Optimal SIC Ordering and Computation Resource Allocation in MEC-Aware NOMA NB-IoT Networks," *IEEE Internet Things J.*, vol. 6, no. 2, pp. 2806-2816, Apr. 2019.

[10] X. Lu, P. Wang, D. Niyato, D. I. Kim, and Z. Han, "Wireless charging technologies: Fundamentals, standards, and network applications," *IEEE Commun. Surveys Tuts.*, vol. 18, no. 2, pp. 1413–1452, 2nd Quart., 2016.

[11] M. Dai, Y. Wu, L. Qian, Z. Su, B. Lin and N. Chen, "UAV-Assisted Multi-Access Computation Offloading via Hybrid NOMA and FDMA in Marine Networks," *IEEE Trans. Netw. Sci. Eng.*, vol. 10, no. 1, pp. 113-127, 1 Jan.-Feb. 2023.

[12] M.-M. Zhao, Q. Shi, and M.-J. Zhao, "Efficiency maximization for UAV-enabled mobile relaying systems with laser charging," *IEEE Trans. Wireless Commun.*, vol. 19, no. 5, pp. 3257–3272, May 2020.

[13] M. Jia, Q. Gao, Q. Guo and X. Gu, "Energy-Efficiency Power Allocation Design for UAV-Assisted Spatial NOMA," *IEEE Internet Things J.*, vol. 8, no. 20, pp. 15205-15215, Oct. 2021.

[14] L. Zhang, Y. Wang, M. Min, C. Guo, V. Sharma and Z. Han, "Privacy-Aware Laser Wireless Power Transfer for Aerial Multi-Access Edge Computing: A Colonel Blotto Game Approach," *IEEE Internet Things J.*, vol. 10, no. 7, pp. 5923-5939, Apr. 2023.

[15] J. Ouyang, Y. Che, J. Xu, and K. Wu, "Throughput maximization for laser-powered UAV wireless communication systems," in *Proc. IEEE ICC Workshops*, May 2018, pp. 1–6.

[16] B. Liu, Y. Wan, F. Zhou, Q. Wu and R. Q. Hu, "Resource Allocation and Trajectory Design for MISO UAV-Assisted MEC Networks," *IEEE Trans. Veh. Technol.*, vol. 71, no. 5, pp. 4933-4948, May 2022.

[17] M. El-Emary, A. Ranjha, D. Naboulsi and R. Stanica, "Energy-Efficient Task Offloading and Trajectory Design for UAV-based MEC Systems," in *Int. Conf. Wirel. Mob. Comput. Netw. Commun. (WiMob)*, Montreal, QC, Canada, 2023, pp. 274-279.

[18] J. Ji, K. Zhu, C. Yi and D. Niyato, "Energy Consumption Minimization in UAV-Assisted Mobile-Edge Computing Systems: Joint Resource Allocation and Trajectory Design," *IEEE Internet Things J.*, vol. 8, no. 10, pp. 8570-8584, May 2021.

[19] C. Liu, Y. Zhong, R. Wu, S. Ren, S. Du and B. Guo, "Deep Reinforcement Learning Based 3D-Trajectory Design and Task Offloading in UAV-Enabled MEC System," *IEEE Trans. Veh. Technol.*, vol. 74, no. 2, pp. 3185-3195, Feb. 2025.

[20] K. Xiang and Y. He, "UAV-Assisted MEC System Considering UAV Trajectory and Task Offloading Strategy," in *IEEE Int Conf Commun*, Rome, Italy, 2023, pp. 4677-4682.

[21] D. Wang, J. Tian, H. Zhang and D. Wu, "Task Offloading and Trajectory Scheduling for UAV-Enabled MEC Networks: An Optimal Transport Theory Perspective," *IEEE Wirel. Commun. Lett.*, vol. 11, no. 1, pp. 150-154, Jan. 2022.

[22] X. Zhang, J. Zhang, J. Xiong, L. Zhou and J. Wei, "Energy-Efficient Multi-UAV-Enabled Multiaccess Edge Computing Incorporating NOMA," *IEEE Internet Things J.*, vol. 7, no. 6, pp. 5613-5627, Jun. 2020.

[23] Y. Lu, H. Zhou, H. Wang, T. Jiang and V. C. M. Leung, "Online Trajectory Optimization and Resource Allocation in UAV-Assisted NOMA-MEC Systems," in *IEEE Int. Workshop Qual. Serv.*, Guangzhou, China, 2024, pp. 1-2.

[24] N. R. Kota and K. Naidu, "Minimizing Energy Consumption in H-NOMA Based UAV-Assisted MEC Network," *IEEE Commun. Lett.*, vol. 27, no. 9, pp. 2536-2540, Sep. 2023.

[25] Z. Liu, J. Qi, Y. Shen, K. Ma and X. Guan, "Maximizing Energy Efficiency in UAV-Assisted NOMA–MEC Networks," *IEEE Internet Things J.*, vol. 10, no. 24, pp. 22208-22222, Dec. 2023.

[26] Z. Liu, X. Liu, V. C. M. Leung and T. S. Durrani, "Energy-Efficient Resource Allocation for Dual-NOMA-UAV Assisted Internet of Things," *IEEE Trans. Veh. Technol.*, vol. 72, no. 3, pp. 3532-3543, Mar. 2023.

[27] Y. He, Y. Gan, H. Cui and M. Guizani, "Fairness-Based 3-D Multi-UAV Trajectory Optimization in Multi-UAV-Assisted MEC System," *IEEE Internet Things J.*, vol. 10, no. 13, pp. 11383-11395, Jul. 2023.

[28] Y. Du, K. Yang, K. Wang, G. Zhang, Y. Zhao and D. Chen, "Joint Resources and Workflow Scheduling in UAV-Enabled Wirelessly-Powered MEC for IoT Systems," *IEEE Trans. Veh. Technol.*, vol. 68, no. 10, pp. 10187-10200, Oct. 2019.

[29] Q. Li, L. Shi, Z. Zhang and G. Zheng, "Resource Allocation in UAV-Enabled Wireless-Powered MEC Networks With Hybrid Passive and Active Communications," *IEEE Internet Things J.*, vol. 10, no. 3, pp. 2574-2588, Feb. 2023.

[30] Y. Gao, F. Lu, P. Wang, W. Lu, Y. Ding and J. Cao, "Resource Optimization of Secure Data Transmission for UAV-Relay Assisted Maritime MEC System," in *IEEE Int Conf Commun*, Rome, Italy, 2023, pp. 3345-3350.

[31] W. Lu et al., "Secure NOMA-Based UAV-MEC Network Towards a Flying Eavesdropper," *IEEE Trans. Commun.*, vol. 70, no. 5, pp. 3364-3376, May 2022.

[32] X. Qin, Z. Song, T. Hou, W. Yu, J. Wang and X. Sun, "Joint Optimization of Resource Allocation, Phase Shift, and UAV Trajectory for Energy-Efficient RIS-Assisted UAV-Enabled MEC Systems," *IEEE Trans. Green Commun. Netw.*, vol. 7, no. 4, pp. 1778-1792, Dec. 2023.

[33] J. Tian, D. Wang, H. Zhang and D. Wu, "Service Satisfaction-Oriented Task Offloading and UAV Scheduling in UAV-Enabled MEC Networks," *IEEE Trans. Wirel. Commun.*, vol. 22, no. 12, pp. 8949-8964, Dec. 2023.

[34] Z. Han, T. Zhou, T. Xu and H. Hu, "Joint User Association and Deployment Optimization for Delay-Minimized UAV-Aided MEC Networks," *IEEE Wirel. Commun. Lett.*, vol. 12, no. 10, pp. 1791-1795, Oct. 2023.

[35] Y. Wang and J. Chen, "Poster: Towards Constraint-Based Model Repair to Ensure Multiple Mission Objectives in UAV-Enabled MEC Systems for Disaster Response and Rescue," in *Proc. - IEEE Int. Conf. Mobil., Oper., Serv. Technol.,*, Dallas, TX, USA, 2024, pp. 275-277.

[36] Q. Tang, Y. Yang, H. Yang, D. Cao and K. Yang, "Energy Consumption Minimization for Hybrid Federated Learning and Offloadable Tasks in UAV-Enabled WPCN," *IEEE Trans. Netw. Sci. Eng.*, vol. 11, no. 5, pp. 4639-4650, Sep.-Oct. 2024.

[37] S. Zhou, H. Yang, L. Xiang and K. Yang, "Temporal-Assisted Beamforming and Trajectory Prediction in Sensing-Enabled UAV Communications," *IEEE Trans. Commun.*, vol. 73, no. 7, pp. 5408-5419, Jul. 2025.

[38] T. Irum, M. Usman Ejaz and M. Elkashlan, "Minimizing Task Offloading Delay in NOMA-MEC Wireless Systems," in *Proc. - IEEE Glob. Power, Energy Commun. Conf.*, Nevsehir, Turkey, 2022, pp. 632-637.

[39] F. Fang, Y. Xu, Z. Ding, C. Shen, M. Peng and G. K. Karagiannidis, "Optimal Resource Allocation for Delay Minimization in NOMA-MEC

Networks," *IEEE Trans. Commun.*, vol. 68, no. 12, pp. 7867-7881, Dec. 2020.

[40] X. Huang, S. Zeng, D. Li, P. Zhang, S. Yan and X. Wang, "Fair Computation Efficiency Scheduling in NOMA-Aided Mobile Edge Computing," *IEEE Wirel. Commun. Lett.*, vol. 9, no. 11, pp. 1812-1816, Nov. 2020.

[41] H. Qiu, S. Gao, Y. Chen and G. Tu, "Energy-Efficient Rate Allocation for NOMA-MEC Offloading Under Outage Constraints," *IEEE Commun. Lett.*, vol. 26, no. 11, pp. 2710-2714, Nov. 2022.

[42] J. Li, F. Wu, K. Zhang and S. Leng, "Joint Dynamic User Pairing, Computation Offloading and Power Control for NOMA-based MEC System," in *Int. Conf. Wirel. Commun. Signal Process.*, Xi'an, China, 2019, pp. 1-6.

[43] L. Lin, W. Zhou and Z. Zhao, "Analytical Modeling of NOMA-Based Mobile Edge Computing Systems With Randomly Located Users," *IEEE Commun. Lett.*, vol. 24, no. 12, pp. 2965-2968, Dec. 2020.

[44] B. Liu, C. Liu and M. Peng, "Resource Allocation for Energy-Efficient MEC in NOMA-Enabled Massive IoT Networks," *IEEE J. Sel. Areas Commun.*, vol. 39, no. 4, pp. 1015-1027, Apr. 2021.

[45] Q. Han, G. Zheng and C. Xu, "Energy-Efficient Resource Allocation for Mobile Edge Computing in NOMA-Enabled Small Cell Networks," in *Int. Conf. Commun. Technol. Proc.*, Nanning, China, 2020, pp. 415-419.

[46] M. Zeng, N. -P. Nguyen, O. A. Dobre and H. V. Poor, "Delay Minimization for NOMA-Assisted MEC Under Power and Energy Constraints," *IEEE Wirel. Commun. Lett.*, vol. 8, no. 6, pp. 1657-1661, Dec. 2019.

[47] Y. Cai, Z. Zhang, Y. Huang, W. Yu, X. Nie and H. Liu, "Cooperative Resource Allocation for NOMA-MEC Multi-Cell Network," *IEEE Trans. Veh. Technol.*, Jan. 22, 2025, doi: 10.1109/TVT.2025.3532648.

[48] Z. Ding, J. Xu, O. A. Dobre and H. V. Poor, "Joint Power and Time Allocation for NOMA–MEC Offloading," *IEEE Trans. Veh. Technol.*, vol. 68, no. 6, pp. 6207-6211, Jun. 2019.

[49] Y. Dursun, F. Fang and Z. Ding, "Hybrid NOMA based MIMO offloading for mobile edge computing in 6G networks," *China Commun.*, vol. 19, no. 10, pp. 12-20, Oct. 2022.

[50] W. Huang and Z. Ding, "New Insight for Multi-User Hybrid NOMA Offloading Strategies in MEC Networks," *IEEE Trans. Veh. Technol.*, vol. 73, no. 2, pp. 2918-2923, Feb. 2024.

[51] Z. Ding, D. Xu, R. Schober and H. V. Poor, "Hybrid NOMA Offloading in Multi-User MEC Networks," *IEEE Trans. Wirel. Commun.*, vol. 21, no. 7, pp. 5377-5391, July 2022.

[52] B. Su, Q. Ni, W. Yu and H. Pervaiz, "Optimizing Computation Efficiency for NOMA-Assisted Mobile Edge Computing With User Cooperation," *IEEE Trans. Green Commun. Netw.*, vol. 5, no. 2, pp. 858-867, Jun. 2021.

[53] L. Shi, Y. Ye, X. Chu and G. Lu, "Computation Energy Efficiency Maximization for a NOMA-Based WPT-MEC Network," *IEEE Internet Things J.*, vol. 8, no. 13, pp. 10731-10744, Jul. 2021.

[54] P. Liu, J. Wang, K. Ma and Q. Guo, "Joint Cooperative Computation and Communication for Demand-Side NOMA-MEC Systems With Relay Assistance in Smart Grid Communications," *IEEE Internet Things J.*, vol. 11, no. 19, pp. 30594-30606, Oct. 2024.

[55] Y. Zhang, H. Zhang, Y. Li, Y. Zhang and S. Yuan, "Joint Resource Allocation and Task Offloading for Hybrid NOMA-assisted MEC Network with Network Slicing," in *Int. Conf. Commun. Technol. Proc.*, Pyeongchang, Korea, Republic of, 2023, pp. 164-170.

[56] J. Du, H. Wu, M. Xu and R. Buyya, "Computation Energy Efficiency Maximization for NOMA-Based and Wireless-Powered Mobile Edge Computing With Backscatter Communication," *IEEE. Trans. Mob. Comput.*, vol. 23, no. 6, pp. 6954-6970, Jun. 2024.

[57] X. Yang, H. Lu, F. Guo, Y. Wang, C. Kong and Q. Lu, "Joint Grouping and Offloading in NOMA-Assisted Multi-MEC IoVT Systems," in *Proc. - IEEE Glob. Commun. Conf.*, Rio de Janeiro, Brazil, 2022, pp. 5699-5704.

[58] J. Liu, X. Zhao, P. Qin, S. Geng, Z. Chen and H. Zhou, "Learning-Based Multi-UAV Assisted Data Acquisition and Computation for Information Freshness in WPT Enabled Space-Air-Ground PIoT," *IEEE Trans. Netw. Sci. Eng.*, vol. 11, no. 1, pp. 48-63, Jan.-Feb. 2024.

[59] Y. Zeng, S. Chen, Y. Cui, J. Yang and Y. Fu, "Joint Resource Allocation and Trajectory Optimization in UAV-Enabled Wirelessly Powered MEC for Large Area," *IEEE Internet Things J.*, vol. 10, no. 17, pp. 15705-15722, Sep. 2023.

[60] G. Li, M. Zeng, D. Mishra, L. Hao, Z. Ma and O. A. Dobre, "Latency Minimization for IRS-Aided NOMA MEC Systems With WPT-Enabled IoT Devices," *IEEE Internet Things J.*, vol. 10, no. 14, pp. 12156-12168, Jul. 2023.

[61] Y. Yang, Y. Gong and Y. -C. Wu, "Energy-Sensitive Binary Offloading for Reconfigurable-Intelligent-Surface-Assisted Wireless-Powered Mobile-Edge Computing," *IEEE Internet Things J.*, vol. 11, no. 7, pp. 11593-11605, Apr. 2024.

[62] L. Zhang, Q. Song, M. Wu, W. Qi and L. Guo, "Joint Terminal Pairing and Multi-Dimensional Resource Allocation for Cooperative Computation in a WP-MEC System," *IEEE Trans. Green Commun. Netw.*, vol. 7, no. 3, pp. 1447-1456, Sep. 2023.

[63] F. Wang, J. Xu and S. Cui, "Optimal Energy Allocation and Task Offloading Policy for Wireless Powered Mobile Edge Computing Systems," *IEEE Trans. Wirel. Commun.*, vol. 19, no. 4, pp. 2443-2459, Apr. 2020.

[64] M. Bolourian and H. Shah-Mansouri, "Energy-Efficient Task Offloading for Three-Tier Wireless-Powered Mobile-Edge Computing," *IEEE Internet Things J.*, vol. 10, no. 12, pp. 10400-10412, Jun. 2023.

[65] L. Zhang, H. Yang, Y. Zhao and J. Hu, "Joint Port Selection and Beamforming Design for Fluid Antenna Assisted Integrated Data and Energy Transfer," *IEEE Wirel. Commun. Lett.*, vol. 13, no. 7, pp. 1833-1837, Jul. 2024.

[66] W. Zhu, X. Chen, L. Jiao, G. Min and Y. Wang, "NOMA-Based WPT-MEC Network System Cost Efficient Units Minimization," in *IEEE Int. Conf. Comput. Commun.,* Chengdu, China, 2022, pp. 1086-1091.

[67] J. Han, G. H. Lee, S. Park and J. K. Choi, "Joint Subcarrier and Transmission Power Allocation in OFDMA-Based WPT System for Mobile-Edge Computing in IoT Environment," *IEEE Internet Things J.*, vol. 9, no. 16, pp. 15039-15052, Aug. 2022.

[68] A. Al-Hourani, S. Kandeepan and S. Lardner, "Optimal LAP Altitude for Maximum Coverage," *IEEE Wireless Commun. Lett.*, vol. 3, no. 6, pp. 569-572, Dec. 2014.

[69] F. H. Panahi and F. H. Panahi, "Reliable and energy-efficient UAV communications: A cost-aware perspective," *IEEE Trans. Mobile Comput.*, vol. 23, no. 5, pp. 4038–4049, May 2024.

[70] Z. Yang, Z. Ding, P. Fan and N. Al-Dhahir, "A General Power Allocation Scheme to Guarantee Quality of Service in Downlink and Uplink NOMA Systems," *IEEE Trans. Wirel. Commun.*, vol. 15, no. 11, pp. 7244-7257, Nov. 2016.

[71] C. Liu, M. Ding, C. Ma, Q. Li, Z. Lin, and Y.-C. Liang, "Performance analysis for practical unmanned aerial vehicle networks with LoS/NLoS transmissions," in *Proc. IEEE Int. Conf. Commun. Workshops*, Kansas City, MO, USA, 2018, pp. 1–6.

[72] A. Meng, X. Gao, Y. Zhao, and Z. Yang, "Three-dimensional trajectory optimization for energy-constrained UAV-enabled IoT system in probabilistic LoS channel," *IEEE Internet Things J.*, vol. 9, no. 2, pp. 1109–1121, Jan. 2022.

[73] A. Naouri, H. Wu, N. A. Nouri, S. Dhelim and H. Ning, "A Novel Framework for Mobile-Edge Computing by Optimizing Task Offloading," *IEEE Internet Things J.*, vol. 8, no. 16, pp. 13065-13076, Aug. 2021.

[74] F. Guo, H. Zhang, H. Ji, X. Li and V. C. M. Leung, "Joint Trajectory and Computation Offloading Optimization for UAV-assisted MEC with NOMA," *IEEE Conf. Comput. Commun. Workshops*, Paris, France, 2019, pp. 1-6.

[75] S. Boyd and L. Vandenberghe, *Convex Optimization.* Cambridge, U.K.: Cambridge Univ. Press, 2004.

[76] M. C. Grant and S. P. Boyd. (Dec. 2018). *CVX: MATLAB Software for Disciplined Convex Programming.* [Online]. Available: http://web.cvxr.com/cvx/doc/CVX.pdf.

[77] C. Ye and Y. Cui, "Stochastic Successive Convex Approximation for General Stochastic Optimization Problems," *IEEE Wireless Commun. Lett.*, vol. 9, no. 6, pp. 755-759, Jun. 2020.

[78] Wu, L. Dai, S. Dou and Y. Xia, "Accelerated Successive Convex Approximation for Nonlinear Optimization-Based Control," *IEEE Trans. Autom. Control*, doi: 10.1109/TAC.2025.3555375.

[79] S. Zhao, T. Zhang, S. Ma, and M. Chen. "Dandelion optimizer: A nature-inspired metaheuristic algorithm for engineering applications," *Eng. Appl. Artif. Intell.*, vol. 114, pp. 105075, Sep. 2022.

[80] S. Suyanto, A. A. Ariyanto, and A. F. Ariyanto. "Komodo mlipir algorithm," *Appl. Soft. Comput.*, vol. 114, pp. 108043, Jan. 2022.

[81] M. Alimohammadi and T. M. R. Akbarzadeh. "State-space adaptive exploration for explainable particle swarm optimization," *Swarm Evol. Comput.*, vol. 94, pp. 101868, Apr. 2025.

[82] L. Si, X. Zhang, Y. Tian, S. Yang, L. Zhang and Y. Jin, "Linear Subspace Surrogate Modeling for Large-Scale Expensive Single/Multiobjective Optimization," *IEEE Trans. Evol. Comput.*, vol. 29, no. 3, pp. 697-710, Jun. 2025.

[83] H. Gu, H. Wang and Y. Jin, "Surrogate-Assisted Differential Evolution With Adaptive Multisubspace Search for Large-Scale Expensive Optimization," *IEEE Trans. Evol. Comput.*, vol. 27, no. 6, pp. 1765-1779, Dec. 2023.

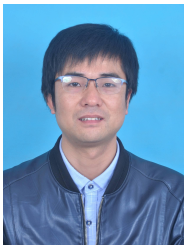

Xuecai Bao received the B.S. degree from Northeast Forestry University, Harbin, China, in 2005, and the M.S. and Ph.D. degrees from Harbin Institute of Technology, Harbin, China in 2007 and 2014, respectively.

He is currently post-doctoral researcher at Nanjing University of Posts and Telecommunications and an a Professor with School of Information and Engineering, Jiangxi University of Water Resources and Electric Power. From September 2017 to September 2018, he was a visiting scholar with University of Alberta, Canada. His research interests include resource management for wireless sensor network and wireless network, Edge/Fog computing, and IoT. Email: lx97821@juwp.edu.cn/lx97821@nit.edu.cn

Fugui Liu received the B.S. degree from Anyang Institute of Technology, Anyang, China, in 2023.

He is currently a Master student in the school of Information Engineering at Jiangxi University of Water Resources and Electric Power. His research interests include Resource allocation in wireless networks and Edge computing.

Fenghui Zhang received the Ph.D. degree from the Information and Communication Engineering, Southeast University, Nanjing, China, in 2023.

He is currently an Associate Professor with the College of Electronic and Information Engineering, West Anhui University. He has been a Visiting Scholar with the Institute of Technology, Dublin, Ireland, and the University of Alberta, Alberta, Canada, in 2013 and 2017, respectively. He has published over 30 papers in the areas of edge computing and mobile communications. His research interests include mobile-edge computing and vehicular network. He serves as an Editor of International Journal of Wireless Communications and Mobile Computing, and he also serves as a reviewer of several IEEE transactions and journals. E-mail: 03000072@wxc.edu.cn

Kun Yang received his PhD from the Department of Electronic & Electrical Engineering of University College London (UCL), UK.

He is currently a Chair Professor in the School of Computer Science & Electronic Engineering, University of Essex, UK, leading the Network Convergence Laboratory (NCL). He is also an affiliated professor of Nanjing University. His main research interests include wireless networks and communications, future Internet and edge computing. In particular he is interested in energy aspects of future communication systems such as 6G, promoting energy self-sustainability via both energy efficiency (green communications and networking) and energy harvesting (wireless charging). He has managed research projects funded by UK EPSRC, EU FP7/H2020, and industries. He has published 400+ papers and filed 20 patents. He serves on the editorial boards of a number of IEEE journals (e.g., IEEE ComMag, TNSE, WCL). He is a Deputy Editor-in-Chief of IET Smart Cities Journal. He is a Distinguished Lecturer of IEEE ComSoc. He has been a Judge of GSMA GLOMO Award at World Mobile Congress – Barcelona since 2019. He is a Member of Academia Europaea (MAE), IEEE Fellow, IET Fellow, and an ACM Distinguished Scientist.